EXTENSIONS OF ONE-DIMENSIONAL TOPOLOGICAL INSULATOR MODELS AND THEIR PROPERTIES

A THESIS SUBMITTED TO

THE GRADUATE SCHOOL OF ENGINEERING AND SCIENCE

OF BILKENT UNIVERSITY

IN PARTIAL FULFILLMENT OF THE REQUIREMENTS FOR

THE DEGREE OF

MASTER OF SCIENCE

IN

PHYSICS

By

Yetkin Pulcu

April 2021

Extensions of one-dimensional topological insulator models and their properties
By Yetkin Pulcu
April 2021

We certify that we have read this thesis and that in our opinion it is fully adequate, in scope and in quality, as a thesis for the degree of Master of Science.

Balázs Hetényi(Advisor)

Oğuz Gülseren

Seçkin Kürkçüoğlu

Approved for the Graduate School of Engineering and Science:

Ezhan Karaşan
Director of the Graduate School

ABSTRACT

EXTENSIONS OF ONE-DIMENSIONAL TOPOLOGICAL INSULATOR MODELS AND THEIR PROPERTIES

Yetkin Pulcu
M.S. in Physics
Advisor: Balázs Hetényi
April 2021

We mainly study the SSH model, a one dimensional topological insulator. As a start, we give a brief introduction about the model and theoretically showed that it should have at least 2 distinct states using Jackiw-Rebbi model. Instead of using only the periodic boundary conditions, we also use open boundary conditions which revealed the zero energy edge states. Introducing the spectral symmetries, we show how a given system can be characterized using the periodic table of topological insulators [1] and depending on the symmetries we discuss which invariant can be used to determine different topological states. Using an enlarged system for a certain symmetry class $\mathbb{Z}$, we show that polarization or Berry phase fails to distinguish different topological states. Subsequently, we implement a similar idea that Haldane used [2], breaking the time-reversal symmetry via introducing the complex next nearest neighbor hopping and find that the system is characterized by $\mathbb{Z}_2$ invariant. Moving away from the "textbook" way of writing the Bloch states, we introduce the distance dependent SSH model where the distance between A and B sublattice is p/q with p and q are being co-primes. We find that the polarization can be found using the inversion symmetry of the wannier centers, which characterize the topological index. Plotting the curve in the parameter space, we come to conclusion that Brillouin zone must be extended q times in order for the system to conserve its periodicity, which brings the knot behaviour of the curves that can be used to distinguish the topological state. At last, we make the SSH model spinful by introducing the time-reversal symmetry protecting Rashba spin-orbit coupling. Due to the Kramers' theorem, degenerate states occur and non-Abelian Berry connection must be constructed to analyze the system. We find that Kato propagator is suitable and gauge invariant way of doing this and computed the time-reversal polarization of the system.

Keywords: Topological insulators, Electric polarization, Topological phase transitions, Berry connection, Kato propagator.

ÖZET

TEK BOYUTLU TOPOLOJIK YALTKAN MADDELERIN UZANTLAR VE ÖZELLIKLERI

Yetkin Pulcu
Fizik, Yüksek Lisans
Tez Danışmanı: Balázs Hetényi
Nisan 2021

Çalışmanın genelinde, bir boyutlu topolojik bir yalıtkan olan SSH modeli incelendi. İlk olarak, modelin neden en az 2 farklı topolojik durumunun olabileceği, Jackiw-Rebbi modeli kullanılarak teorik olarak gösterildi. Periyodik sınır koşulları yerine, açık sınır koşulları kullanılarak sistemde sıfır enerjili durumlar olduğu gösterildi. Spektral simetriler gösterildikten sonra, herhangi bir sistemin nasıl kategorize edilebileceği topolojik yalıtkanların periyodik tablosuna [1] göre gösterildi. Topolojik değişmezlerin neler olabileceği analiz edilerek bunlardan bazılarının sarım sayısı ve elektrik polarizasyon olabileceği gösterildi. Daha sonra, genişletilmiş bir SSH modeli kullanılarak $\mathbb{Z}$ invaryantlı sistemlerin özelliklerinin polarizasyon metoduyla bulunamayacağı kanıtlandı. Haldane'in [2] fikrini bir boyuta uyarlayarak, zaman simetrisini kıran, kompleks bir sonraki en yakın komşuya sıçrama genliği sisteme dahil edildi ve sonucunda sistemin $\mathbb{Z}_2$ invaryantı ile tasvir edilebileceği gösterildi. Bir sonraki bölümde, ders kitaplarının genel olarak kabul ettiği Bloch fonksiyonlarından uzaklaşıp, aralarında p/q kadar mesafe olan A ve B yerleri belirlendi. Bu sistem, Wannier fonksiyonlarının ters çevirme simetrisini koruması nedeniyle, elektrik polarizasyonu ile tanımlanabilir ve bu sayede topolojik indeksi de ortaya çıkarılabilir. Bu bilgiler kullanılarak parametrik uzayda çizlen eğrinin kendi üzerine tekrar dönebilmesi için, sistemin q kadar uzatılması gerektiği gösterildi ve bu uzatmanın düğüm teorisi ile ilgili bağları incelendi. Son olarak, SSH modeline spin eklemek için Rashba spin-yörünge etkileşimi göz önünde bulunduruldu. Sistem, Kramers teoremi yüzünden dejanere özdurumlar içerir ve bu yüzden Abelyan olmayan Berry fazı hesaplanmak zorundadır. Bu nedenle, Kato ilerleticisi tartışıldı ve spinli sistemlerin Berry fazlarını bulabilmek için iyi bir aday olduğu gösterildi ve zaman simetrisine uygun polarizasyon hesaplandı ve sistemin topolojik özellikleri bulundu.

Anahtar sözcükler: Topolojik yalıtkanlar, Elektrik polarizasoyun, Topolojik faz

geçişleri, Berry fazı, Kato yayıcısı.

Acknowledgement

First of all, I should thank to Professor Hetényi for such an enjoyable thesis journey. I learned a lot from him and he always treated me as his peer which means a lot in terms of gaining confidence. I should also thank Professor Oktel and Professor Bulutay for their guidance through my undergraduate and graduate years. I thoroughly enjoyed every class I took from them. There were many friends whom I enjoyed talking through my Bilkent years but I cannot list every one of them here and I hope they know themselves. But I should mention Tahoora and Selçuk whose companionship and support cannot be underestimated in this pandemic. We almost spend a year together and I will remember it with a smile on my face. I thank to my family, whose support is beyond my imagination and expectation. I haven't seen them for a year and their patience and love is more than enough for me. Lastly, my friends from Bilkent Scientific Communication Society made the covid time enormously enjoyable. I am very lucky to know them.

Dedicated to my family; Birgül, Fahri and Deniz...

Contents

List of Figures

List of Tables

Chapter 1

Introduction

1.1 An overview

Two branches, topology and condensed matter physics, that looks completely different at first look, was merged in 1980s by the work of Klaus von Klitzing [5] in which he experimentally discovered the quantum Hall effect and the work done by Thouless et al.[6] in which they showed that Hall conductance, or now commonly known as TKNN invariant, that can be identified via Chern number in the Brillouin zone. Later, it is understood that, TKNN integer is connected to Berry phase, or a geometric phase acquired after the cyclic and adiabatic evolution, which is discovered by Michael Berry in 1984 [7]. Duncan Haldane, 6 years later after TKNN, connected the quantum hall effect to band theory by proposing a model with broken time-reversal symmetry which is now known as $\mathbb{Z}$ invariant [2]. In 1989, Zak showed that, non-trivial Berry phase can be observed in one-dimensional Brillouin zone due to the torus type of geometry [8]. Around the same time, physicists raised an issue about the polarization in the periodic systems, in which they claimed that, polarization cannot be measured. King-Smith-Vanderbilt [9] and Resta [10] resolved the issue using the Zak phase and they created the modern theory of electric polarization. The next breakthrough came in 2005, where Kane and Mele [11] showed that, breaking the time-reversal

symmetry is not necessary for the observation of the non-trivial topology. However, the proposal is failed experimentally at first sight because it is proposed for graphene and its spin-orbit coupling is not high enough to show the effect. A different model called BZH, is introduced by Bernevig, Hughes and Zhang which has a similar behaviour that Kane and Mele proposed but former has a stronger spin-orbit interaction and thus observed in HgTe/CdTe quantum well [12]. Due to the increasing number of discoveries regarding with the $\mathbb{Z}$ and $\mathbb{Z}_2$ labels, using the symmetries of the Hamiltonian, a periodic table of the topological insulators and superconductors are invented. [3] [13] [14].

1.2 Structure of the Thesis

In order to investigate the topological band theory, we first give the necessary background in the chapter 2 that contains 2-level SSH model, dispersion relation of the hamiltonian in the open and periodic boundary conditions, how to determine the topological index from the symmetries of the system, derivation of the Berry phase that Resta introduced [15] instead of the textbook definition, the ambiguity of the Berry phase in one dimension, modern theory of the polarization and the relation with the Berry phase, the generalization of the Berry phase or so-called Wilson loop and finally the winding number which is necessary to calculate the topological index $\mathbb{Z}$. Using these calculation tools, we start to analyze different models based on SSH model. In chapter 3, we still consider the distance-independent hamiltonian but with the additional diagonal term. We analyze how introducing such diagonal terms change the topological behaviour of the system based on the symmetry analysis and Berry phase calculations introduced in chapter 2. At the end of the chapter, we show how adding a second nearest neighbor (or even more distant neighbors hoppings) hopping affect the topology. In chapter 4, we start to analyze how the distance between A and B sublattices affect the topology of the system by introducing a complex NNN hopping. In order to determine the behaviour, we use the table introduced in chapter 2 and calculate the Wilson loop of the system. Switching to parameter space, we show that in order to keep the periodicity of the system, 1st Brillouin zone

must be extended and this extension brings a different topological invariant, that is knot invariant. We further justify the knot invariant by considering the winding numbers of the knots. Until here, all the analysis was done for the spinless fermions. However, in order to make the problem more physical, in chapter 5, we introduce the spinful SSH model with Rashba spin-orbit coupling. Due to the presence of the time-reversal symmetry, we discuss the Kramers' theorem, how it brings the degeneracy to the system and using it, we define the time-reversal polarization. In order to make the numerical calculation gauge free, we discuss Kato propagator and show that it is just a projection of the occupied bands in the thermodynamic limit. Using it, we define Wilson loop in terms of the Kato propagator and calculate the topological invariant $\mathbb{Z}_2$ of the system.

Chapter 2

SSH Model

In 1979, a seminal paper appeared in Physical Review Letters, written by Su, Schrieffer and Heeger [16] where they investigated long-chain polyenes. Although it is a very minimalist model, it was later understood that, the contribution of this toy model to topological physics is huge. The model investigates the polyacetylene, a one dimensional material with carbon atoms but with an altering bonds between them, classified as a one-dimensional topological insulator with edge states.

In the most generic way, using the second quantization, the SSH Hamiltonian can be written as [17],

$$H = \sum_{n=1}^{N} (t + \delta t) c_n^\dagger d_n + \sum_{n=1}^{N-1} (t - \delta t) c_{n+1}^\dagger d_n + h.c \tag{2.1}$$

where $c_n^\dagger$ and c_n are the creation and annihilation operators respectively and N is the number of unit cells. They act on A sublattice. Similarly, d_n and $d_n^\dagger$ act on B sublattice. As it can be understood from the hamiltonian, the SSH model is a bi-partite model, where particle-hole symmetry, which will be discussed with other two symmetries, may appear.

The hopping amplitude within the same unit cell is denoted by $(t + \delta t)$ and

between neighboring unit cells is $(t - \delta t)$. When $\delta t > 0$, the bond between A and B in the same unit cell is shorter than the neighbouring unit cell, making the former more stronger. As it can be understood from the sign of δt, it appears that, there might be two phases of SSH model, a trivial topology and a non-trivial topology, which we will investigate later.

We can Fourier transform Eq. (2.1), in order to work in the periodic k-space. We define the Fourier transformed annihilation and creation operator as,

$$c_n = \frac{1}{\sqrt{N}} \sum_k e^{-ikna} c_k \tag{2.2}$$

$$d_n = \frac{1}{\sqrt{N}} \sum_k e^{-ikna} d_k. \tag{2.3}$$

The hermitian conjugate of these operators can be taken in a normal way. Putting Eq. (2.2) and Eq. (2.3) to Eq. (2.1), we obtain

$$H = \frac{(t+\delta t)}{N} \sum_n \sum_k \sum_{k'} e^{ikna} c_k^\dagger e^{-ik'na} d_{k'} + \frac{(t-\delta t)}{N} \sum_n \sum_k \sum_{k'} e^{ik(n+1)a} c_k^\dagger e^{-ik'na} d_{k'} + h.c, \tag{2.4}$$

where $k, k' \in 1st$ BZ. We can simplify Eq. (2.4) by exploiting the fact that, for the SSH model, there is no distance between the A and B sublattice in the same unit cell. Therefore, simply looking at the first part of the Eq. (2.4), we can realize the delta function in the form of

$$\sum_n \sum_k \sum_{k'} e^{i(k-k')na} = N\delta_{kk'}. \tag{2.5}$$

Applying the same procedure to all of the terms in Eq. (2.4), we obtain the following hamiltonian

$$H = \sum_k (c_k^\dagger d_k^\dagger) \underbrace{\begin{pmatrix} 0 & t+\delta t+(t-\delta t)e^{-ik} \\ t+\delta t+(t-\delta t)e^{ik} & 0 \end{pmatrix}}_{\mathrm{H(k)}} \begin{pmatrix} c_k \\ d_k \end{pmatrix}. \tag{2.6}$$

Since there is no next-nearest neighbor (NNN) hopping or on-site potential, diagonal axis only consist of zeros. Re-naming things just for convention, we have $J = t + \delta t$ and $J' = t - \delta t$. We can easily find the eigenvalues of $H(k)$ as,

$$E(k) = \pm\sqrt{J^2 + J'^2 + 2JJ'cosk}. \tag{2.7}$$

The gap closure occurs when $J = J'$ with $k = \pm\pi$. Using Eq. (2.7), we can plot how the energy of the system changes with respect to k. We take natural energy unit to be J and J'.

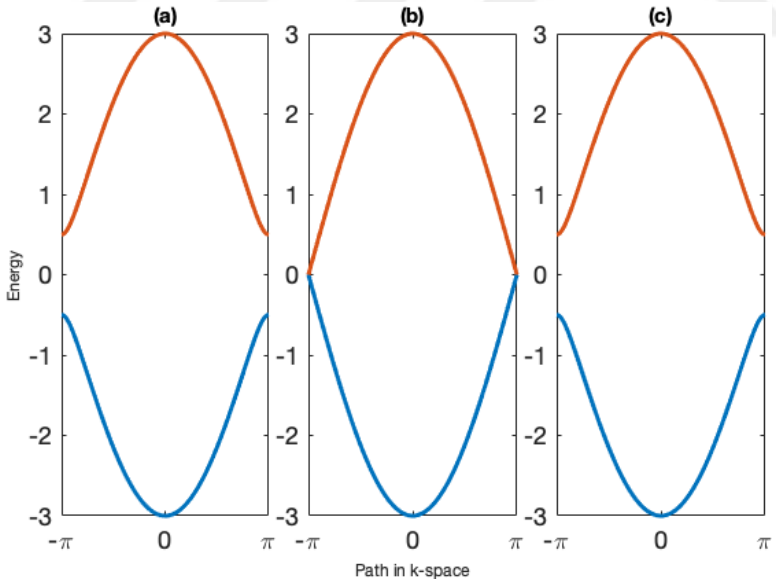

Figure 2.1: Dispersion relation of the SSH model with different hopping values. Fig. 2.1.A shows $J = 1.25$ and $J' = 1.75$. Fig. 2.1.B shows $J = J'$ and Fig. 2.1.C shows $J = 1.75$, $J' = 1.25$

From Fig. 2.1, one can mistakenly conclude that, since Eq. (2.6) looks symmetric, and changing the value of J to J' and J' to J has no effect on the system as their band energy plots are exactly same. However, this conclusion, as we will show later is not correct. Although their bulk energies are similar, in order to

change Fig. 2.1.A to Fig. 2.1.C, we have to close the gap and re-open it, which actually changes the topology of the system.

Moving away from the periodic boundary conditions(PBC), where Fig. 2.1 is plotted, we now consider the open boundary conditions(OBC). As we observed that, changing one of the hopping constants, like J in the range of $J > J'$ to $J' > J$, we see that band gap closes, and re-opens. Fig. 2.2 is the band energy of the same system where we used OBC in order to investigate the edge states of the system.

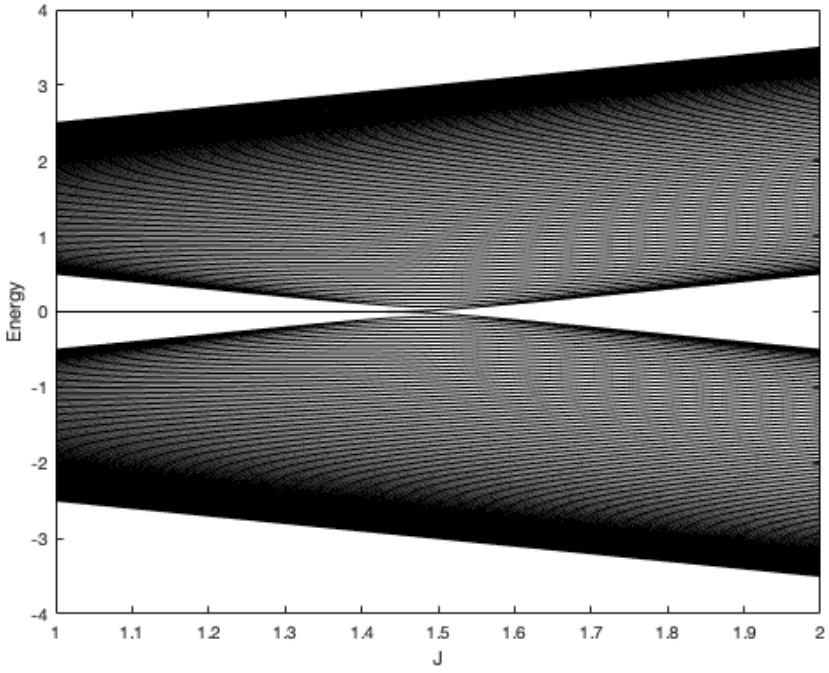

Figure 2.2: SSH model in the open boundary conditions with $J' = 1.5$ and 100 unit cell. Zero energy states appear for $J' > J$

One can directly see the interesting conclusion in the Fig. 2.2. When $J' > J$, we see there are zero energy states, whereas $J > J'$ has none. The transition occurs when $J \sim J'$ as we predicted in the PBC version of the same plot. Before plotting the edge states, we analytically show that, there are two topologically distinct states in the SSH model using the Jackiw-Rebbi Model.

2.1 Jackiw-Rebbi Model

The existence of zero modes is important in order to understand how the edge states behave. Such zero modes are generally protected by the specific kind of discrete symmetries, which will be examined later on. In 1976, Jackiw and Rebbi [18] found such zero modes in one-dimensional field theory. Here we implemented the ideas of Jackiw-Rebbi to SSH model, which gives some analytical insight.

Starting from the Eq. (2.6) and writing the $H(k)$ near the gap closure k point such that $k = k_0 + dk$ with $k_0 = \pi$, the interaction Hamiltonian can be written as,

$$H(k) = [t + \delta t + (t - \delta t)cos(\pi + dk)]\sigma_x + (t + \delta t)sin(\pi + dk)\sigma_y. \tag{2.8}$$

Using the approximations $cos(\pi + dk) = -1$ and $sin(\pi + dk) = -dk$ and disregarding small terms, we can write the Hamiltonian as,

$$H(k) = 2\delta t\sigma_x - tdk\sigma_y. \tag{2.9}$$

Changing from discrete k-space to continuous position space, $dk \to -i\delta_x$ we can write the continuum Hamiltonian as,

$$H = 2\delta t\sigma_x + it\delta_x\sigma_y. \tag{2.10}$$

As we are looking the zero energy modes, the equation that has to be solved is $H\Psi(x) = 0$. Therefore, we have

$$(2\delta t\sigma_x + it\delta_x\sigma_y)\Psi(x) = 0. \tag{2.11}$$

In order to get rid of at least one Pauli matrix, we multiply Eq. (2.11) by σ_x and arranging the differential equation, it yields the solution as,

$$\Psi(x) = \Psi(0)\exp\left(\int_0^x \pm\frac{2\delta t(x')}{t}dx'\right). \tag{2.12}$$

We can choose the sign of $\delta t(x)$ to be positive when $x > 0$ and negative when $x < 0$. Therefore, in order to have a normalized solutions,the $\pm$ ambiguity of the integral can be dismissed an we can take the solution as $\sigma_z \Psi = -\Psi$

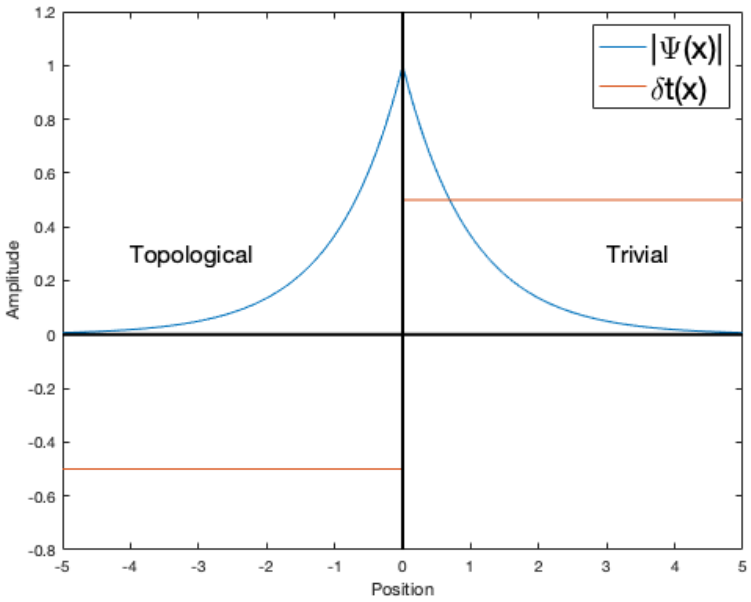

Figure 2.3: The zero energy solution of $\Psi(x)$, when $\delta t < 0$, SSH model is in topological state and $\delta t > 0$ corresponds to trivial state. Phase transition occurs when $\delta t = 0$

As it can be seen from Fig. 2.3, the wave-function can only be normalized when the sign of δt changes at the boundary. This is another clue that different topological states might exist in the SSH model.

2.2 Topological Insulators in a Ten Fold Way

Similar to periodic table of elements in topological physics, there is also a periodic table [3], [13], smaller than the original, where we can understand how the given system behaves, depending on the three discrete symmetries. Through this chapter, we introduce different ways of attacking the given Hamiltonian, either analytically or using computer power. However, one of the most crucial tool to

use is discrete symmetries. Using these symmetries, we can almost always tell how the topology enters the physics of the system. In order to make topological classification rigorous, here we introduce three discrete symmetries, whose existence are in the hearth of topological phases of quantum matter.

2.2.1 Time Reversal Symmetry

Time reversal symmetry, as it will be shown in this chapter, is represented by an anti-unitary operator [19]. A time-reversal symmetric system can be thought of as, whenever the time has reversed, the physical quantities of the system remain intact. As it can be observed that, the known universe cannot be time-reversal invariant system due to entropy. Intuitively, the position is even under the time-reversal. Therefore, we can write $\mathcal{T}x\mathcal{T}^{-1} = x$ which suggests that the observable position and time-reversal operator commutes. We can also write the same thing for momentum, but they now anti-commute, $\mathcal{T}p\mathcal{T}^{-1} = -p$. Therefore, looking at the canonical commutation relation $[x, p] = i\hbar$, we can write,

$$\mathcal{T}[x, p]\mathcal{T}^{-1} = -[x, p] = -i\hbar \tag{2.13}$$

where the minus sign comes from the fact that momentum and $\mathcal{T}$ anti-commute. So, the time-reversal operator changes the sign of the imaginary number, therefore is anti-unitary. In the most general form, $\mathcal{T} = \mathcal{U}\mathcal{K}$ where $\mathcal{U}$ is the unitary part and $\mathcal{K}$ is the complex conjugation. For the Bloch Hamiltonian, then, we can write the commutation relation as,

$$\mathcal{T}H(k)\mathcal{T}^{-1} = H(-k), \tag{2.14}$$

since we know that momentum has to change sign. Writing in a unitary way, then, the Eq. (2.14) reads,

$$\mathcal{U}H^*(k)\mathcal{U}^{-1} = H(-k). \tag{2.15}$$

For the spinless models, $\mathcal{U}^2 = \mathbf{1}$.[1] Taking a generic Hamiltonian in the form $H(k) = d_x(k)\sigma_x + d_y(k)\sigma_y + d_z(k)\sigma_z$ and using the fact that, for spinless model, $\mathcal{T}$ can be taken as complex conjugation operator,

$$\begin{aligned} d_x(k) &= d_x(-k), \\ d_y(k) &= -d_y(-k), \\ d_z(k) &= d_z(-k). \end{aligned} \tag{2.16}$$

The minus sign in the d_y part is due to the fact that σ_y has imaginary entries. Since SSH hamiltonian can be expressed as $H(k) = (J + J'\cos k)\sigma_x + J'\sin k\sigma_y$, it can be seen that taking $\mathcal{T}$ to be $\mathbf{1}\mathcal{K}$, we can see that it satisfies Eq. (2.16), therefore H_{SSH} has time-reversal symmetry(TRS).

2.2.2 Particle-Hole Symmetry

In general, particle-hole or charge conjugation symmetry is discussed in the topic of superconductivity and as the name implies, it changes the filled and empty states. From the BCS theory, cooper pair, a pair of electrons, can be broken apart. Therefore, electrons can be created and annihilated. In general, the Hamiltonian describes this phenomena can be written as,

$$\mathcal{H} = \sum_{nm} H_{nm} c_n^\dagger c_m + \tfrac{1}{2}(\Delta_{nm} c_n^\dagger c_m^\dagger + \Delta_{nm}^* c_m c_n), \tag{2.17}$$

where $c_n^\dagger$ and c_n are the creation and annihilation operators respectively. Then the BdG Hamiltonian can be written as,

$$\mathcal{H} = \frac{1}{2} C^\dagger H_{\mathrm{BdG}}\, C \tag{2.18}$$

and in the matrix form H_{BdG} can be written as,

[1] As it should be remarked here, SSH model is spin independent and we don't study Kramer's theorem here, but later on when spinful model is investigated.

$$H_{\mathrm{BdG}} = \begin{pmatrix} H & \Delta \\ -\Delta^* & -H^* \end{pmatrix}. \tag{2.19}$$

Although we don't investigate the superconductivity, particle-hole symmetry(PHS) can also be found in bi-partite topological insulators. In k space, then, acting with $\mathcal{C}$ on H_{BdG} can be represented as,

$$\mathcal{C}H_{BdG}(k)\mathcal{C}^{-1} = -H_{BdG}(-k). \tag{2.20}$$

We should note here that, $\mathcal{C}$ is an anti-unitary operator as is $\mathcal{T}$. From the Eq. (2.20), the energy spectrum of H_{BdG} is symmetric with respect to zero energy. In the case of H_{SSH}, $\mathcal{C}$ can be taken as $\sigma_z\mathcal{K}$ such that,

$$\begin{aligned} (\sigma_z\mathcal{K})(J + J'cosk)\sigma_x(\mathcal{K}\sigma_z) &= -(J + J'cosk)\sigma_x \\ (\sigma_z\mathcal{K})(J'sink)\sigma_y(\mathcal{K}\sigma_z) &= (J'sink)\sigma_y \end{aligned} \tag{2.21}$$

where we used the fact that $\sigma_z^{-1} = \sigma_z$ and commutation relation $\sigma_a\sigma_b = i\varepsilon_{abc}\sigma_c$.[2] Therefore, Eq. (2.20) is satisfied as the sine is an odd and cosine is an even function.

2.2.3 Chiral Symmetry

Chiral or sub-lattice symmetry is defined with respect to two other symmetries. It is defined as $\mathcal{S} = \mathcal{T}\mathcal{C}$. Therefore, it is needed that either both symmetries exist or both should be absent in the system for chrial symmetry to be present. From the definition, it is an unitary operator in the single-particle space and can be written as $\mathcal{S} = \mathcal{U}_T\mathcal{K}\mathcal{U}_\mathcal{C}\mathcal{K} = \mathcal{U}_T\mathcal{U}_C^*$. Hence, $\mathcal{S}$ is a unitary operator. One of the most important consequence of having a chrial symmetry can be deduced from the anti-commuting behavior of the $\mathcal{S}$ operator.

[2]Since $\mathcal{K}$ only produce non-trivial result when acted on σ_y, we don't show the calculation explicitly.

$$\mathcal{S}H(k)\mathcal{S}^{-1} = -H(k). \tag{2.22}$$

Using the Eq. (2.22), we can write the following equality.

$$\begin{aligned} \mathcal{S}H(k)\left|\Psi\right\rangle &= -H(k)\mathcal{S}\left|\Psi\right\rangle, \\ E(k)\mathcal{S}\left|\Psi\right\rangle &= -H(k)\mathcal{S}\left|\Psi\right\rangle. \end{aligned} \tag{2.23}$$

Therefore, we can see that if $|\Psi\rangle$ is the energy eigenstate with the energy $E(k)$, then $\mathcal{S}|\Psi\rangle$ is also an energy eigenstate with $-E(k)$. Hence, the energy spectrum is symmetric about k-axis, if the system has chiral symmetry, degeneracies occur at $E(k) = 0$

Using the first argument of the existence of the chiral symmetry, since SSH model has both TRS and PHS, as a consequence it also has chiral-symmetry. We can find the $\mathcal{C}$ operator using the $\mathcal{S} = \mathcal{U}_T\mathcal{U}_C^* = \mathbf{1}\sigma_z^* = \sigma_z$. Since H_{SSH} only contains σ_x and σ_y operator, we can see that Eq. (2.22) holds. Therefore, in order for a system to be chrial symmetric, it cannot contain one of the other Pauli matrices. This last deduction will be important when we try to find the index of the topological invariant.

2.2.4 Periodic Table of Topological Insulators

Using the notation of the Ref. [3], we introduce the periodic table for topological insulators and superconductors. One of the usages of the table is that, for the Hamiltonian at hand, it tells which topological index the system has, depending on the discrete symmetries of the Hamiltonian. On the other hand, it also tells that, whether adding terms to the Hamiltonian breaks the certain symmetries, thus changing the index.

As it can be seen from the table[3], there are 3 values for different kind of

[3]Although the table shows the symmetries as $\mathcal{T}, \mathcal{C}$ and $\mathcal{S}$, their values actually corresponds to square of these operators.

				δ							
Class	T	C	S	0	1	2	3	4	5	6	7
A	0	0	0	$\mathbb{Z}$	0	$\mathbb{Z}$	0	$\mathbb{Z}$	0	$\mathbb{Z}$	0
AIII	0	0	1	0	$\mathbb{Z}$	0	$\mathbb{Z}$	0	$\mathbb{Z}$	0	$\mathbb{Z}$
AI	+	0	0	$\mathbb{Z}$	0	0	0	$2\mathbb{Z}$	0	$\mathbb{Z}_2$	$\mathbb{Z}_2$
BDI	+	+	1	$\mathbb{Z}_2$	$\mathbb{Z}$	0	0	0	$2\mathbb{Z}$	0	$\mathbb{Z}_2$
D	0	+	0	$\mathbb{Z}_2$	$\mathbb{Z}_2$	$\mathbb{Z}$	0	0	0	$2\mathbb{Z}$	0
DIII	−	+	1	0	$\mathbb{Z}_2$	$\mathbb{Z}_2$	$\mathbb{Z}$	0	0	0	$2\mathbb{Z}$
AII	−	0	0	$2\mathbb{Z}$	0	$\mathbb{Z}_2$	$\mathbb{Z}_2$	$\mathbb{Z}$	0	0	0
CII	−	−	1	0	$2\mathbb{Z}$	0	$\mathbb{Z}_2$	$\mathbb{Z}_2$	$\mathbb{Z}$	0	0
C	0	−	0	0	0	$2\mathbb{Z}$	0	$\mathbb{Z}_2$	$\mathbb{Z}_2$	$\mathbb{Z}$	0
CI	+	−	1	0	0	0	$2\mathbb{Z}$	0	$\mathbb{Z}_2$	$\mathbb{Z}_2$	$\mathbb{Z}$

Figure 2.4: Periodic table of topological insulators and superconductors. Adapted from [3].

symmetries. $\mathcal{T} = \pm 1$ is when the system has TRS.[4] Similarly, $\mathcal{C}$ having ± 1 when particle-hole symmetry preserved. For $\mathcal{S} = 1$, the system is chiral symmetric. Note that, since $\mathcal{S}$ is a unitary operator, it can only square to 1. For the spatial part, there are again three different indices. These indices are the ones are very important while calculating the topological invariant of the system.

When the invariant is 0, it means that any gapped Hamiltonian can be deformed into each other, without closing the gap, therefore, the edge states if there are any, are not topologically protected.

A $\mathbb{Z}$ invariant is when the topological phases can be classifed as an integer number $0, \pm 1, \pm 2, ...$ There are many mathematical tools to calculate $\mathbb{Z}$ such as Chern number or winding number or some cases, the polarization of the system. As we work in $d = 1$ throughout this thesis, winding number is the most convenient but polarization will also be used.

At last, $\mathbb{Z}_2$ invariant where the topological phases of the system can be classified by 0 and 1. Therefore a $\mathbb{Z}_2$ system can only have 2 different topological phase. It can be calculated using Zak phase, which we will derive in the next section, as,

[4] $\mathcal{T} = -1$ corresponds to spinful systems. For spinless, it can only squared to $+1$

$$\gamma = \frac{1}{\pi} \int_{1stBZ} dk \, \langle \Psi | \, i\partial_k \, | \Psi \rangle \, . \tag{2.24}$$

2.3 Winding Number and Polarization as a Topological Invariant in SSH Model

As we introduced the ten-fold symmetry of topological insulators and found the symmetry operators of SSH model with $\mathcal{T} = \mathbf{1}\mathcal{K}$, $\mathcal{C} = \sigma_z\mathcal{K}$ and $\mathcal{S} = \sigma_z$, we can see that all of them squares to 1 and according to Fig. 2.4, then, SSH model is classified as BDI and its topological invariant in $d = 1$ is $\mathbb{Z}$, therefore, winding number and polarization can be calculated to find different topological phases. However, we first derive the discrete Berry phase.

2.3.1 Berry Phase and Its Connection to Polarization

Assuming a generic Hamiltonian in the form,

$$H(\lambda) \, |\Psi\rangle = E(\lambda) \, |\Psi\rangle \tag{2.25}$$

where λ is a vector in a quantum system and $|\Psi\rangle$ is ground state wave function. Assuming that there is no degeneracy in the system, the phase difference between two eigenstates at different parameters can be defined as,

$$\exp(-i\varphi_{12}) = \langle \Psi(\lambda_1) | \Psi(\lambda_2) \rangle \tag{2.26}$$

where we assumed that the states are already normalized. Hence, we can write the phase difference between two different parameters as

$$\varphi_{12} = \text{-Imlog}(\, \langle \Psi(\lambda_1) | \Psi(\lambda_2) \rangle \, . \tag{2.27}$$

If we do the above procedure for all φ_{ab} and sum them up and close the curve such that the end point takes the values φ_{n1} with n being the number of eigenstates, we can obtain the phase as,

$$\gamma = \varphi_{12} + \varphi_{23} + ... + \varphi_{n1} \tag{2.28}$$

where γ is the Berry phase of the system. In order to go from discrete to continuous, we can discretize the system, such that Eq. (2.27) looks like,

$$\exp(-i\varphi_{12}) = \langle\Psi(\lambda_1))|\Psi(\lambda_1 + \Delta\lambda)\rangle\,. \tag{2.29}$$

We can Taylor expand the Eq. (2.29), [5]

$$\begin{aligned} 1 - i\varphi = \langle\Psi(\lambda)|\,(|\Psi(\lambda)\rangle + \Delta\lambda\,|\Psi'(\lambda)\rangle) + \mathcal{O}(\Delta\lambda^2), \\ d\varphi = i\,\langle\Psi(\lambda|)\nabla_\lambda\,|\Psi(\lambda)\rangle\,d\lambda. \end{aligned} \tag{2.30}$$

Then taking the closed line integral of the Eq. (2.30), we end up with the Berry phase

$$\gamma = \oint_C d\varphi = i\,\langle\Psi(\lambda)|\,\nabla_\lambda\,|\Psi(\lambda)\rangle\,d\lambda, \tag{2.31}$$

where $i\,\langle\Psi(\lambda|)\nabla_\lambda\,|\Psi(\lambda)\rangle$ is called Berry connection, similar to vector potential in the topic of electromagnetic theory and denoted by $A(\lambda)$. As in the case of electromagnetic theory, Berry connection is not observable which we can show as, taking an arbitrary gauge such that $\widetilde{\Psi} \to \exp(-i\theta(\lambda))\Psi$, where $\theta(\lambda)$ is an arbitrary gauge choice.

$$\begin{aligned} \widetilde{A}(\lambda) &= i\,\langle\widetilde{\Psi}(\lambda)|\,\nabla_\lambda\,|\widetilde{\Psi}(\lambda)\rangle \\ &= i\,\langle\Psi(\lambda|)\nabla_\lambda\,|\Psi(\lambda)\rangle + \frac{d(\theta(\lambda))}{d\lambda} \\ &= A(\lambda) + \frac{d(\theta(\lambda))}{d\lambda}. \end{aligned} \tag{2.32}$$

[5] Expanding the higher $\mathcal{O}$ would give the cumulants like variance.

It is not invariant under gauge transformation, thus, not observable.

We can also write Eq. (2.31) as

$$\widetilde{\gamma} = \int i \langle \widetilde{\Psi}(\lambda)| \left[-i\dot{\theta}(\lambda) |\widetilde{\Psi}(\lambda)\rangle + \nabla_\lambda |\widetilde{\Psi}(\lambda)\rangle\right], \\ \widetilde{\gamma} = \gamma + \int \frac{d(\theta(\lambda))}{d\lambda} d\lambda. \tag{2.33}$$

The last integral can be taken such that, assume $\lambda = 0$ is the initial state and $\lambda = 1$ is the final such that, since the loop is closed, we want $|\widetilde{\Psi}(\lambda = 1)\rangle = |\widetilde{\Psi}(\lambda = 0)\rangle$. Therefore, the last integral becomes $\theta(\lambda = 1) - \theta(\lambda = 0) = 2\pi m$ and we obtain the result as,

$$\widetilde{\gamma} = \gamma + 2\pi m \tag{2.34}$$

where m is an integer. The result shows that, Berry phase is gauge invariant in mod2π. Hence, it is gauge-invariant when thought of as a phase angle as in the case of Eq. (2.26). We are now ready to generalize Berry phase approach to multi-band case, which is known as Wilson loop.

2.3.2 Wilson Loop

In order to go from one band to multi-band case, we need a more general tool to calculate the topological invariant, as many of the systems have more than one occupied bands. To do that, we introduce the projector operator acting on the occupied states.

$$\mathbb{P} = \sum_{a=1}^{n_f} |u^a(k)\rangle \langle u^a(k)| , \tag{2.35}$$

where n_f is the number of occupied bands. Hence, Wilson loop can be written as,

$$W^{ab} = \lim_{N\to\infty} \langle u^a(k_f)| \left[\overline{\prod}_{\{k_i=1:N\}} \mathbb{P}(k_i)\right] |u^b(k_{in})\rangle \tag{2.36}$$

where the bar on top of the product symbol ensures the path dependence of the multiplication since the projector is matrix valued equation with W is being an $n_f \times n_f$ matrix. It is clear from the Eq. (2.36) that, we evaluate the overlaps between the states at different momenta k.

$$\begin{aligned} \langle u^a(k)|u^b(k-\delta k\rangle &= \langle u^a(k)| \left[u^b(k)\rangle - dk\nabla_k u^b(k)\right] \\ &= \delta^{ab} - dk \langle u^a(k)|\nabla_k u^b(k)\rangle \\ &\approx \exp \langle u^a(k)|\nabla_k u^b(k)\rangle \\ &= \exp\left[-dkA^{ab}(k)\right], \end{aligned} \tag{2.37}$$

A^{ab} is called non-Abelian Berry connection. [6] [7] Hence, we can connect the Eq. (2.36) with the Eq. (2.37) as,

$$W(l) = \overline{\exp}\left[-\int dkA(k)\right] \tag{2.38}$$

with l is the path and the necessity of the bar on top of the exponential indicates that A is a matrix valued function.

2.3.3 Modern Theory of Polarization

In the case of classical electrodynamics, dipole moment per unit length can be written as,

$$\mathrm{p} = \frac{1}{a}\sum q_i x_i \tag{2.39}$$

where x_i is the position of the charge q_i. For d = 1, we can see that polarization has the units of charge. This information will be useful when we prove that polarization is not just a bulk property but also an edge property.

[6] i is missing in the definition of Eq. (2.37) compared Eq. (2.31) but this is just a convention, whether A is real or complex.

[7] The reason why we are using the cell periodic functions is explained in Appendix C.

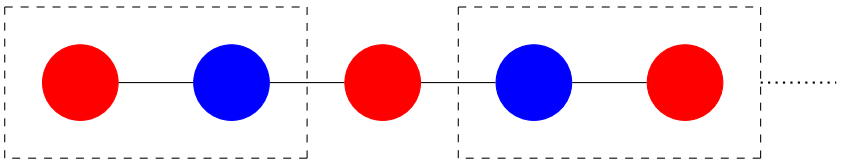

Figure 2.5: A simple d = 1 model with red circles represent the cations and blue circles represent the anions. Anions and cations are spaced by $a/2$. Different choices of unit cells are shown.

Taking a very simplistic one dimensional model as in the Fig. 2.5, calculating the polarization with respect to 1st unit cell gives,

$$\begin{aligned} p &= \frac{1}{a}\left(\frac{a}{4} - \frac{3a}{4}\right), \\ p &= -\frac{1}{2}. \end{aligned} \tag{2.40}$$

Similarly, we can do this for the second unit cell,

$$\begin{aligned} p &= \frac{1}{a}\left(\frac{-a}{4} + \frac{3a}{4}\right), \\ p &= +\frac{1}{2}. \end{aligned} \tag{2.41}$$

As it can be seen that, different choices of unit cells gave different polarization. Therefore, we can conclude that, polarization is not an observable in periodic systems. However, we can also calculate the changes in the polarization. Referring the Fig. 2.5, assume that blue circles(anions), are displaced to the right by δ. Following the same steps, we can calculate the polarization of the system with taking the unit cell as the left one of Fig. 2.5

$$\begin{aligned} p &= \frac{1}{a}\left(\frac{a}{4} - \frac{3a}{4} + \delta\right), \\ p &= -\frac{1}{2} - \frac{\delta}{a}. \end{aligned} \tag{2.42}$$

We can also do the same thing for the second unit cell,

$$\begin{aligned} p &= \frac{1}{a}\left(\frac{-a}{4} - \delta + \frac{3a}{4}\right), \\ p &= +\frac{1}{2} - \frac{\delta}{a}. \end{aligned} \tag{2.43}$$

Now we can calculate the changes in the polarization between Eq. (2.42) with Eq. (2.43)

$$\begin{aligned} p_2 - p_1 &= \frac{-1}{2} + \left(\frac{-\delta}{a}\right) + \frac{1}{2} = \frac{\delta}{a} \rightarrow \text{1st unit cell} \\ p_2 - p_1 &= \frac{1}{2} + \left(\frac{-\delta}{a}\right) - \frac{1}{2} = \frac{\delta}{a} \rightarrow \text{2nd unit cell} \end{aligned} \tag{2.44}$$

Thus, we can conclude that for perodic systems, instead of polarization, the changes in the polarization can be observed. However, the model we discussed here is purely classical where the particles are taken as points. In order improve that, we can treat electrons as quantum mechanical objects and their positions can be represented as the expectation of the positions in a quantum mechanical language $\langle x \rangle = \int \Psi \hat{x} \Psi dx$. In general, x is not bounded and the integral is ill-defined and as shown above shifting the operator by L, a different result can be obtained. Thus, we need to introduce another basis where the states are localized, which is Wannier states. In 1d,

$$|w_{nR}\rangle = \frac{L}{2\pi} \int_{1stBZ} e^{-ikR} |\Psi_{nk}\rangle \, dk. \tag{2.45}$$

Using the Blochs theorem, $\Psi(r) = \exp(ikr)u(r)$ we can find the expectation value of the position using Wannier states.

$$\hat{x} \, |w_{n0}\rangle = \frac{L}{2\pi} \int x e^{ikx} |u(k)\rangle \, dk, \tag{2.46}$$

instead of x operator, we can write $x \rightarrow -i\delta_k$. Eq. (2.46) becomes,

$$\begin{aligned}\hat{x}\,|w_{n0}\rangle &= \frac{L}{2\pi}\int -i\delta_k e^{ikx}\,|u(k)\rangle\,dk,\\ &= \frac{L}{2\pi}\int -i[\delta_k(e^{ikx}\,|u(k)\rangle) - e^{ikx}\delta_k dk\,|u(k)\rangle],\\ &= \frac{L}{2\pi}\int ie^{ikx}\delta_k\,|u(k)\rangle\,dk.\end{aligned} \tag{2.47}$$

From going 2nd equation. to 3rd, we use integration by parts and using the fact that $\exp(ikx)\,|u(k)\rangle$ has the same value at $k = 0$ and $k = \frac{2\pi}{a}$, we found the last integral. Hitting with the $\langle w_{n0}|$, we have

$$\langle w_{n0}|\,\hat{x}\,|w_{n0}\rangle = \frac{1}{2\pi}\int \langle u(k)|\,i\delta_k\,|u(k)\rangle\,dk, \tag{2.48}$$

where we used the fact that, $\langle \xi_k|\psi_{k'}\rangle = \frac{2\pi}{L}\,\langle u_k|v_{k'}\rangle\,\delta(k-k')$ and $L = 1$ Therefore, we showed that Wannier center is just a Berry phase with a constant added. As we mentioned that Wannier centers are the good approximations of the positions of the electrons, we can write Eq. (2.48) as,

$$P_{electric} = \frac{e}{2\pi}\int_{-\pi}^{\pi} \langle u(k)|\,i\delta_k\,|u(k)\rangle\,dk. \tag{2.49}$$

Returning to the Eq. (2.34), we see that since the Polarization can be written as Berry phase divided by 2π, polarization is also gauge invariant in mod m, with m being an integer. This analysis also holds with the classical analysis where we stated that polarization cannot be measured. Here we also make a connection between the projected position operator and the Wilson loop, that is introduced earlier. Defining the new position operator as $\eta = \exp(-2\pi ix/L)$ such that $\langle \Psi_{n,k}|\,\eta\,|\Psi_{n,k'}\rangle = \delta_{k,k+\frac{2\pi}{L}}\,\langle U_{n,k}|U_{n,k+\frac{2\pi}{L}}\rangle$[8]. Therefore, defining the projection operator for the occupied bands as $\mathbb{P} = \sum_k |\Psi(k)\rangle\,\langle\Psi(k)|$, we can write

$$\begin{aligned}\mathbb{P}\eta\mathbb{P} &= \sum_{k,k'} |\Psi(k)\rangle\,\langle\Psi(k)|\,\eta\,|\Psi(k')\rangle\,\langle\Psi(k')|\,,\\ &= \sum_{k} |\Psi(k+\delta k)\rangle\,\langle\Psi(k)|\,.\,\langle u(k+\delta k)|u(k)\rangle\,,\end{aligned} \tag{2.50}$$

[8]The full derivation can be found in Appendix B.

with $\delta k = 2\pi/L$. Defining $\mathbb{P}\eta\mathbb{P}$ as η_P, we can take L^{th} square of η_P,

$$\begin{aligned}\eta_P^L = &\sum_{k,k',k'',...k^{L-1\prime}} |\Psi(k+\delta k)\rangle \langle\Psi(k)|\Psi(k'+\delta k\rangle \langle\Psi(k'|...|\Psi(k^{(L-1)'})+\delta k\rangle \langle\Psi(k^{(L-1)'})|\,. \\ &\langle u(k+\delta k)|u(k)\rangle \langle u(k'+\delta k)|u(k')\rangle ... \langle u((k^{(L-1)'})+\delta k)|u((k^{(L-1)'}))\rangle \\ &= \sum_k \langle u(k+\delta k)|u(k)\rangle \langle u(k)|u(k-\delta k)\rangle ... \langle u(k-(L-2)\delta k)|u(k-(L-1)\delta k)\rangle \\ &|\Psi(k+\delta k\rangle \langle\Psi(k+\delta k| \\ &= \langle u(k+\delta k)|u(k)\rangle \langle u(k)|u(k-\delta k)\rangle ... \langle u(k-2\delta k-2\pi)|u(k-\delta k-2\pi)\rangle .\mathbb{P}\end{aligned} \tag{2.51}$$

where we used the orthogonality of the energy eigenstates $\langle\Psi(k)|\Psi(k'\rangle = \delta_{k,k'}$. Hence, we showed that $\eta_P^L = W\mathbb{P}$, where W is the Wilson loop and $\mathbb{P}$ is the projection operator. This is a crucial equality such that, the eigenvalue of the Wilson loop and the eigenvalue of the $\mathbb{P}\eta\mathbb{P}$ operator is related to each other.

2.3.3.1 Is polarization a bulk property or not ?

As it has been proven that $\mathbb{P}x\mathbb{P}\,|w_{nR}\rangle = x_{wf}\,|w_{nR}\rangle$ by Kivelson [20], instead of using ill-defined electron position in the calculation of the polarization,

$$P = \frac{1}{L}\int_0^L dx x(\rho^{ion} + \rho^{electron}) \tag{2.52}$$

we can use x_{wf} since $|w_{nR}\rangle$ is the closest thing to delta function with, $\delta(x-x_0) = \langle x|x_0\rangle$. Hence, instead of using Eq. (2.52), and taking the positions of the ions as classical, we can write

$$P = \frac{e}{L}\sum_n (x_n^{ion} - x_{n(wf)}^{electron}), \tag{2.53}$$

which just contains the point like charges. Now considering a very long chain like in the Fig. 2.6 where there are three pieces contributing the overall polarization, $P_{total} = P_{start} + P_{bulk} + P_{end}$. Here we can assume a thermodynamic limit in the

bulk such that, $L \approx N = N_b a$ where N_b is the number of unit cells in the bulk and a is the lattice constant. Therefore, for every position, we can write $x_n = na + \tau$. Plugging this into Eq. (2.53) and in the thermodynamic limit, we have

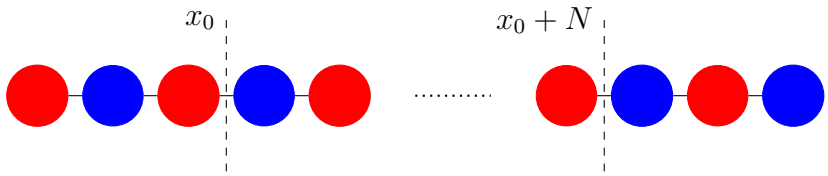

Figure 2.6: A simple d = 1 model in the thermodynamic limit. Blue circles represent the anions and cations are represented by red. Overall region is divided into three parts with the boundaries at x_0 and $x_0 + N$.

$$\begin{aligned} P_{bulk} &= \frac{e}{N_b a} \sum_{n}^{N_b} \left(na + \tau^{ion} - na - \tau^{electron} \right), \\ &= \frac{e}{N_b a} \sum_{n}^{N_b} \left(+\tau^{ion} - \tau^{electron} \right), \\ &= \frac{e}{a} \left(\tau^{ion} - \tau^{electron} \right). \end{aligned} \tag{2.54}$$

We can proceed similarly for the P_{start} and P_{end} regions, but since we have extended the bulk to thermodynamic limit, we assume that all the ions and electrons contributing P_{start} is sitting at exactly x_0 and similarly for the end region, they sit at $x_0 + N$. Thus, we can write,

$$P_{start} = \frac{e}{L} x_0 \left(\#^{ion}_{start} - \#^{electron}_{start} \right), \tag{2.55a}$$

$$P_{end} = \frac{e}{L} \left(x_0 + N_b a \right) \left(\#^{ion}_{end} - \#^{electron}_{end} \right). \tag{2.55b}$$

Since the whole system is neutral and by the construction, the bulk region is neutral, we can conclude that $\#^{ion}_{start} - \#^{electron}_{start} = -\left(\#^{ion}_{end} - \#^{electron}_{end} \right)$. So that we can find $P_{start} + P_{end}$ as,

$$\begin{aligned} P_{start} + P_{end} &= \frac{e}{L} \left(N_b a \right) \left[-\#^{electron}_{start} - \#^{ion}_{start} \right] \\ &= e \left(\#^{electron}_{start} - \#^{ion}_{start} \right) \end{aligned} \tag{2.56}$$

which is charge times a number, as we have also found in Eq. (2.49), which says $P = \frac{\gamma}{2\pi}$ mod m such that real space and k-space is in complete agreement. But

as Eq. (2.56) also states, polarization is not a bulk property, it depends on the edge states.

Returning to the SSH model, as we have stated that, it holds the topological index of $\mathbb{Z}$, we can calculate it through the polarization.

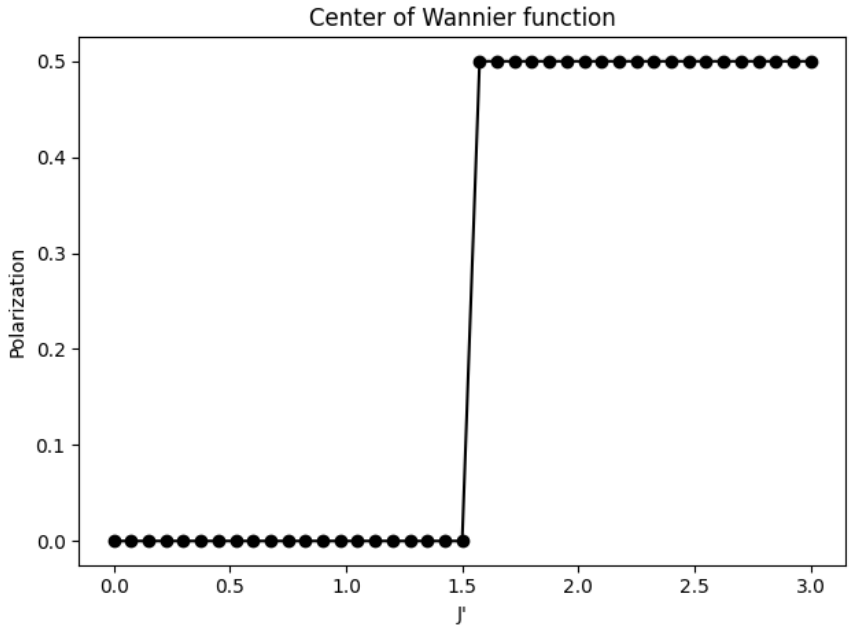

Figure 2.7: Polarization vs J' with J = 1.5. As J'=J, the phase transition occurs and polarization jumps to 0.5. At $J = J'$ it is undefined.

As it can be understood from Fig. 2.7, there are two different values of Berry phase, $\gamma = 0$ and $\gamma = \pi$. Therefore, the polarization takes 2 distinct values. Considering the extreme case where $J = 0$ and $J' \neq 0$, SSH model have 2 edge states in which they decay exponentially towards the bulk that can be seen in Fig. 2.8. Hence, the system has non-zero polarization, opposite of the trivial case where $J' = 0$ with $J \neq 0$ where no edge states are observed. As we have mentioned that, polarization, although a good indicator of phase transitions, is not always enough to be sure that the topology of the system is changed. Considering a model where it contains SSH model polarization with $P = 1$, as we have mentioned that, polarization is gauge invariant mod m, $P = 0$ and $P = 1$ case are basically the same thing. Therefore, polarization is a good indicator when there are two distinct states, but is not a helpful one when there are more

than two. Hence, we use the polarization when the topological index is $\mathbb{Z}_2$ where there are only two different phases.

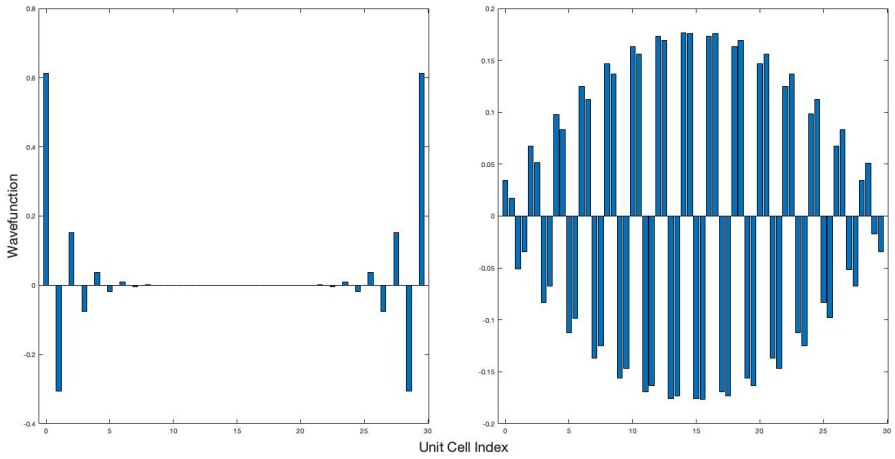

Figure 2.8: (Left) Zero energy edge states of the SSH model with $J = 0.5$ and $J' = 1.5$. (Right) SSH model in the trivial phase with $J = 1$ and $J' = 0.5$.

2.3.4 Winding Number

When we discussed chiral symmetry for $d = 1$ systems, we established a general Hamiltonian where, in order to have a chiral symmetry, one of the three pauli matrices should be absent because of the Eq. (2.22). Then, one of the three coefficients, $d_x(k), d_y(k)$ or $d_z(k)$ should be absent. So we can write the eigenvalue equation of SSH model as,

$$\begin{aligned} H(d) &= d_x\sigma_x + d_y\sigma_y \\ &\Updownarrow \\ H(d)^2 &= d^2\sigma_0 \end{aligned} \tag{2.57}$$

where d can be thought as a parameter like λ as we have discussed before. From Eq. (2.57), it can be deduced that, the vector d swaps only $d_x - d_y$ plane. Therefore, we can define the winding number as, how many times does $d(k)$ wind the origin. There are 2 different ways of calculating the winding number: Graphically and analytically.

2.3.4.1 Graphical Winding Number

Since we established that SSH model has 2 different phases for $J' > J$ and $J' < J$, we can plot the Eq. (2.57) in order to see how many times the $d(k)$ vector winds the origin.

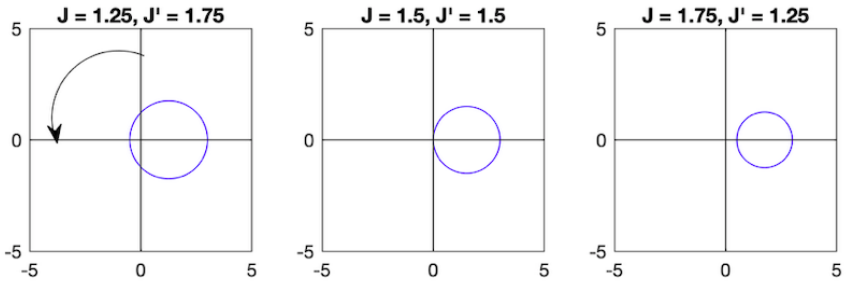

Figure 2.9: Winding number for different intracell/intercell hopping. First case where the winding number $\nu = -1$, refers the topological state. When $J = J'$, ν is undefined. $\nu = 0$ corresponds to topologically trivial state. The arrow shows the orientation of the winding number.

As the Fig. 2.9 shows, SSH model has two different topological states. Trivial case has the winding number $\nu = 0$ whereas topological case has $\nu = -1$. However, one should be careful about the orientations of the winding number. For Fig. 2.9, as the arrow indicates, it is counterclockwise, so we take it to be -1. If there would be a case where it winds in the clockwise, it would count as 1 and they correspond to different topological states. Thus, for an arbitrary shape, in order to find the winding number ν, we need to sum up the number of clockwise winding and number of anti-clockwise winding. Hence, we can write

$$\nu = \nu_{\text{clockwise}} + \nu_{\text{anti-clockwise}}. \tag{2.58}$$

As an example, we give a 2d projection of a trefoil knot, which we will investigate in the further chapters.

As it can be seen from the Fig. 2.10, $\nu = -2$ as both curve winds the origin anti-clockwise. For simplistic curves, the graphical approach is more suitable

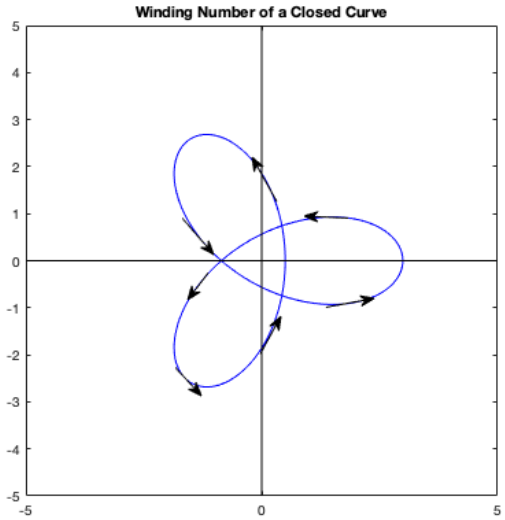

Figure 2.10: Winding number for a 2d projected trefoil knot. The curve winds the origin twice as both of them are anti-clockwise.

as it does not contain evaluating complex integrals. However, we also show the analytical calculation of the winding number.

2.3.4.2 Analytical Winding Number

When the system is one dimensional and has chrial symmetry, the given Hamiltonian can be represented only using σ_x and σ_y matrices

$$H(k) = \begin{pmatrix} 0 & h(k) \\ h^{\dagger}(k) & 0 \end{pmatrix}. \tag{2.59}$$

Then the winding number ν can be represented via,

$$\nu = \frac{1}{2\pi i} \int_0^{2\pi} dk \frac{d}{dk} \log h(k)). \tag{2.60}$$

We also know from SSH model, $h(k)$ has the form of $J + J'\exp(-ik)$. Therefore, as k evolves from 0 to $2\pi/a$, $\exp(-ik)$ also evolves in the complex unit circle. So, we can solve the Eq. (2.60) in the complex plane, taking $z = \exp(ik)$

$$\begin{aligned} \nu &= \frac{1}{2\pi i} \oint dz \frac{d}{dz} \log \text{ h(z)}, \\ &= \frac{1}{2\pi i} \oint dz \frac{h'(z)}{h(z)}. \end{aligned} \tag{2.61}$$

The integral in Eq.(2.61) can be evaluated from Cauchy's argument principle. According the the theorem,

$$\nu = Z - P \tag{2.62}$$

where Z is the number of zeros, and P is the number of poles $f(z)$ inside the contour. Using open form of h(k), we can write

$$h(z) = J + \frac{J'}{z}. \tag{2.63}$$

As it can be seen, z = 0 is the pole of $h(z)$. In order to find, if any, the zeros, we need to solve the Eq. (2.63).

$$\begin{aligned} 0 &= J + \frac{J'}{z}, \\ z &= \frac{-J'}{J}. \end{aligned} \tag{2.64}$$

We know that $z = \exp(ik) \Rightarrow |z| = 1$. Therefore, if $J' > J$, Eq. (2.64) does not hold and h(z) does not have zeros inside the contour. Hence, using Eq. (2.62), ν = -1, since there is one pole and no zeros. Notice that, we found $\nu = -1$ from the graphical winding number too. In case of these values do not agree, we can always change the graphical counting where clockwise and anti-clockwise changes their sign. Only important rule to follow is, one should use the convention through the calculation and do not change in the middle of it. We can also look at if Eq. (2.64) holds for the values where $J > J'$. Indeed it holds and number of zeros inside the contour is 1 so that $\nu = 0$.

As we have showed from various attacking tools, there exist a trivial and topological case of SSH model and since the existence of edge states are protected by chiral symmetry with a topological index of $\mathbb{Z}$, it can be concluded that, the

topology has changed when the deformation from $J > J'$ to $J' > J$ occurs. We conclude this longer chapter by stating that, one can add another terms to H_{SSH} as long as they respect to symmetries of it. Breaking a symmetry, the topological index of the system changes according to the Fig. 2.4. We will investigate such terms in the preceding chapters.

Chapter 3

SSH Model with Next-Nearest Neighbor Hopping

Through the chapter 2, we investigated various tools to categorize the SSH model. Although it was not a new study, it gives perspective how to attack other problems. In this chapter, we investigate two different NNN hoppings, calculate its topological index, edge states and polarization. Instead of re-writing everything, we mostly refer back to chapter 2 for necessary equations and plots.

3.1 Real NNN Hopping

As it was discussed in the previous chapter, SSH model only contains nearest-neighbor hopping, leaving the off-diagonal elements zero in the Eq. (2.6). This time we add NNN terms such that,

$$H = \sum_{n=1}^{N} (t + \delta t) c_n^\dagger d_n + \sum_{n=1}^{N-1} [(t - \delta t) c_{n+1}^\dagger d_n + K_1 c_i^\dagger c_{i+1} - K_2 d_i^\dagger d_{i+1} + h.c]. \quad (3.1)$$

Therefore, Fourier transforming this equation, we obtain,

$$H = (c_k^\dagger d_k^\dagger) \underbrace{\begin{pmatrix} 2K_1 cosk & t+\delta t+(t-\delta t)e^{-ik} \\ t+\delta t+(t-\delta t)e^{ik} & -2K_2 cosk \end{pmatrix}}_{\text{H(k)}} \begin{pmatrix} c_k \\ d_k \end{pmatrix} \tag{3.2}$$

when K_1 = -K_2, we have next nearest hopping with equal amplitudes to both directions. Therefore, we can write

$$H(k) = d_0(k)\sigma_0 + d_x(k)\sigma_x + d_y(k)\sigma_y, \tag{3.3}$$

where $d_i's$ are the coefficients of Pauli matrices, obtained by Eq. (3.2). Because of the σ_0 matrix, the particle hole symmetry is now broken since,

$$\mathcal{C}H_{SSH+NNN}(k)\mathcal{C}^{-1} \neq -H_{SSH+NNN}(-k) \tag{3.4}$$

This can be shown by, taking the same $\mathcal{C}$ opeartors as in the SSH model, $\sigma_z K$, and act on the $d_0\sigma_0$ part of the H,

$$\begin{aligned} \sigma_z\mathcal{K}\ (2Kcosk\sigma_0)\ \mathcal{K}\sigma_z &= 2Kcosk \\ 2Kcosk &\neq -2Kcos(-k). \end{aligned} \tag{3.5}$$

Hence, PHS is broken. TRS preserved since $\mathcal{T}$ can be taken as $\mathbf{1}\mathcal{K}$, which satisfies $\mathcal{K}H_{SSH+NNN}\mathcal{K} = H(-k)$. Because PHS is broken and TRS is preserved, from the definition of the chiral symmetry, it does not exist. From the Fig. 2.4, then, the system is in AI class, which is trivial in d = 1 case. However, when the Berry phase of the system is calculated, there is a discrete jump in the phase near $J = J'$, which can be seen from Fig. 3.1.

In order to resolve this issue, we have to define another symmetry, called inversion symmetry.

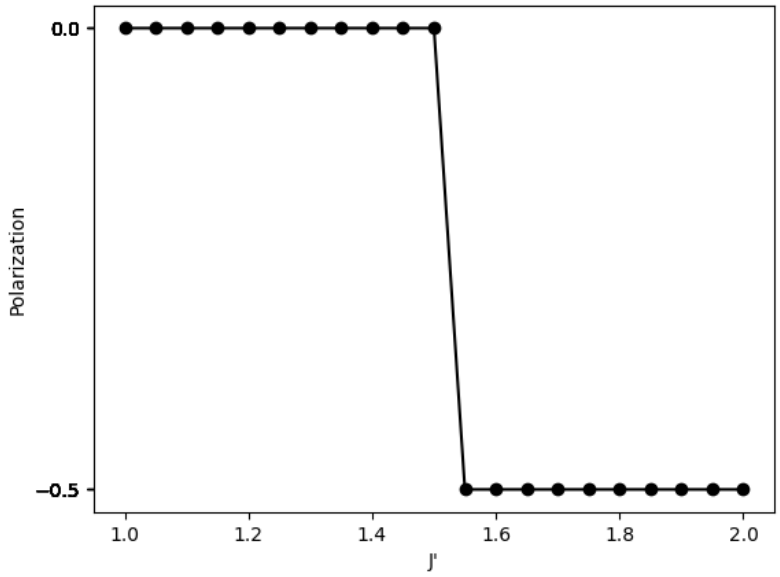

Figure 3.1: Polarization of the SSH model with real next nearest neighbor hopping with changing J'. As it can be seen, although the model is trivial according to periodic table of topological insulators, it has a non-zero bulk polarization for $J' > J$

3.1.1 Inversion Symmetry

The possible nonspatial symmetries of the Hamiltonian of the system has already been discussed in chapter 2: time-reversal symmetry, particle-hole symmetry and chiral symmetry. However, there are other type of symmetries which are called spatial symmetries like inversion symmetry which we discuss here. The heuristic definition can be made as the following; if the system is invariant under inversion symmetry, we can write $x \to -x$. For crystal momentum it also flips the sign and we can write it as,

$$\mathbf{\Pi} H(k) \mathbf{\Pi}^{-1} = H(-k) \tag{3.6}$$

with $\mathbf{\Pi}$ is being a unitary and a non-local operator. Checking the SSH model with on-site potential, it can be easily seen that, the system preserves the inversion symmetry with $\mathbf{\Pi} = \sigma_x$. Because the Wilson loop changes under the inversion

as,

$$\begin{aligned} \mathbf{\Pi} W_{k:0\to 2\pi}(k)\mathbf{\Pi}^{-1} &= W_{k:2\pi\to 0}(-k) \\ &= W^{\dagger}_{k:0\to 2\pi}(-k). \end{aligned} \tag{3.7}$$

Thus, using the Eq. (3.7), with the Wilson loop eigenvalues, we can conclude that $\theta(k) = -\theta(-k)$ such that $\theta = 0$ or π. It can be deduced that, for one-band insulators in d = 1, inversion symmetry acts like $\mathbb{Z}_2$ invariant so that the polarization is quantized to 0 when $J > J'$ and to 1/2 for $J' > J$. Hence, for the systems with inversion symmetry, the table in Ref. [14] should be used and according to table, SSH model with on-site potential falls into AI^2 which is topological and characterized by $M\mathbb{Z}$ or so called mirror winding number.

Another possible method to see that the Berry phase of the system is same with or without the on-site potential is that, σ_0 term does not affect the eigenstates of the system so that Berry phase stays unchanged.

Instead of using real NNN hopping, we can replace it with on-site potential such that Eq. (3.3) recovered and the symmetries of the system is same as in the case of the examined system above. We just need to replace d_0 parameter of σ_0 term such that $2K\cos k \to \Delta$ with Δ is the on-site potential.

As it can be seen from Fig. 3.2 that, both systems have edge states but according to the symmetry analysis, they do not have chiral symmetry to protect the edge states. However, chiral symmetry operator σ_z still relates the even and odd chiral partners on the left figure such that $|\langle edge_{even}|\,\Gamma\,|edge_{odd}\rangle| = 1$ with

$$\Gamma = \underbrace{\mathcal{S}\oplus\mathcal{S}\oplus ...\oplus\mathcal{S}}_{\mathrm{L}} \tag{3.8}$$

where L is the number of unit cells. The reason why Γ still acts like a chiral symmetry operator is that, on-site potential Δ just lifts the energy bands by Δ and the system is now symmetric not with respect to $E = 0$ but $E = \Delta$. However, the figure on the right has $|\langle edge_{even}|\,\Gamma\,|edge_{odd}\rangle| = 0.866 < 1$ which we can conclude that, there is no chirality in the system and increasing the value of K,

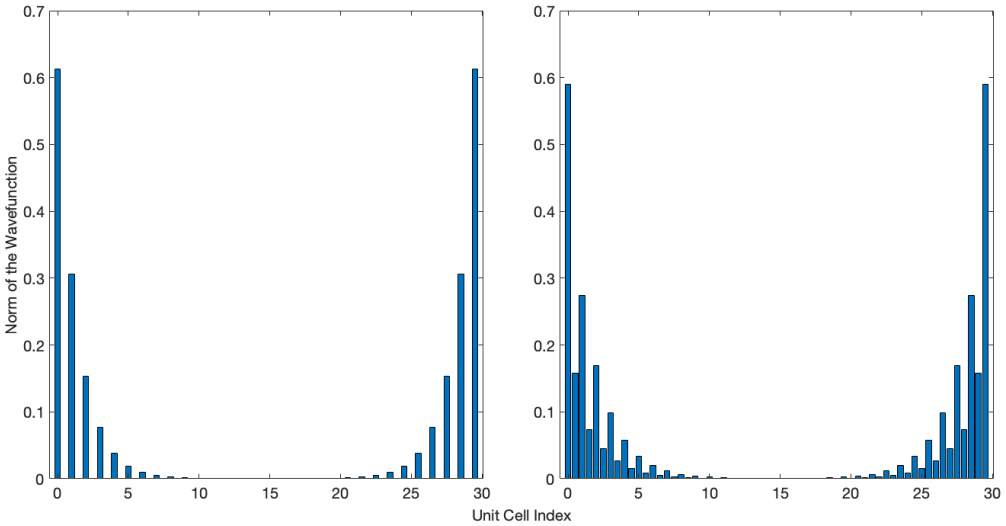

Figure 3.2: Left figure shows the edge states with J = 1, J' = 2 and $\Delta = 1$ and right figure shows the edge states with J = 1, J' = 2 and K = 0.5

the product $|\langle edge_{even}|\,\Gamma\,|edge_{odd}\rangle|$ shrinks more. Although the systems totally have the same symmetries, the edge states behaves differently and the relation between bulk and boundary, called bulk-boundary correspondence, is not direct. However, we can safely say that, because of the eigenvalues of the Wilson loop need to satisfy the condition $\theta(k) = -\theta(-k)$, it can be concluded that two phases, topological and trivial, appears in the system due to the inversion symmetry.

Taking $K_1 = K_2$, we can write the Bloch hamiltonian as,

$$H(k) = d_x(k)\sigma_x + d_y(k)\sigma_y + d_z(k)\sigma_z. \tag{3.9}$$

Since diagonal entries differs by a minus sign, instead of σ_0, we have σ_z, as we pointed out in the chapter where chiral symmetry is discussed, at least one of the three Pauli matrices should be absent in order a system to be chiral symmetric. Hence, σ_z term breaks the symmetry. As the TRS is still preserved with $\mathcal{T} = \mathbf{1}\mathcal{K}$, particle-hole symmetry is also broken and the system is again classified as AI. Therefore, we can generalize that, any even hopping[1] breaks the particle-hole

[1]The contribution to diagonal elements in Eq. (3.2) is called even hoppings. An electron hopes from a sublattice to same sublattice, either in the same unit cell or a different one.

symmetry in extended SSH model. The generalized version of this is investigated by Li et al. [21], where they claim that, $K_1 = K_2$ type of hopping preserves the particle-hole symmetry, which we have shown to be the opposite. Any real even hopping breaks the PHS and chiral symmetry. Furthermore, they also claimed that, fixed NNN hoppings do not lead the topologically non-trivial case, which we also proved to be wrong, since $K_1 = -K_2$ case has the polarization value of 0 and 1/2 which is protected by the inversion symmetry.

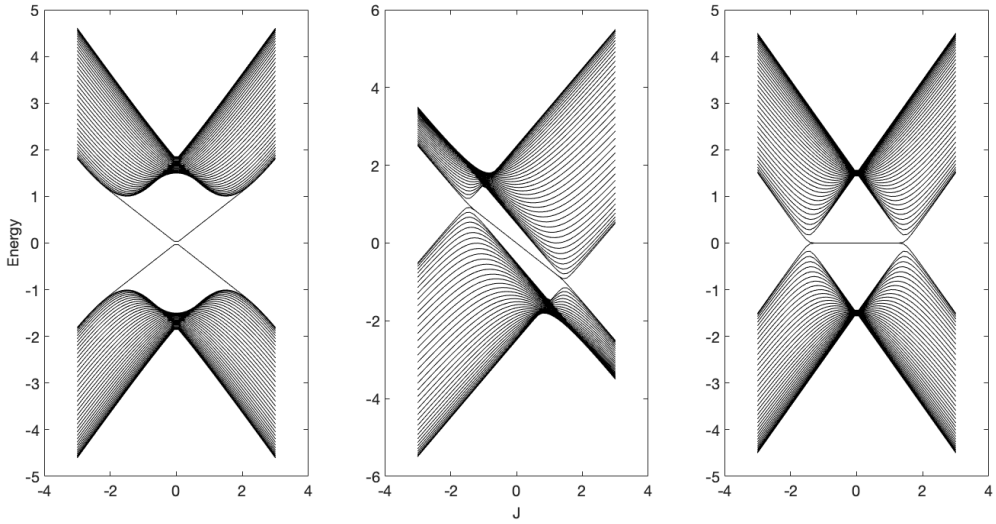

Figure 3.3: Left plot shows the real NNN hoppings with $K_1 = K_2$, middle plot shows the case when $K_1 = -K_2$, and the right plot is the SSH model. For all plots, we used $J' = 1.5$ with $K = 0.5$. The calculations are done for 40 unit cells with the open boundary conditions.

Fig. 3.3 shows couple of SSH models with NNN hoppings. The left plot does not have a gap closure and as we have found above, it does not provide any non-trivial topology, due to the fact that it only has time-reversal symmetry and categorized as AI. Middle plot in Fig. 3.3 is interesting. Although it has zero energy modes, they are not chiral partners of each other because of the real NNN hopping. However, inversion symmetry stays intact and the model has non-trivial topology.

3.2 Complex NNN Hopping

As we have shown in the last section, adding an even real hopping brings topologically distinct states. We can also observe non-trivial topology with following the path Duncan Haldane introduced in 1980s for graphene [2]. In order to break the time-reversal symmetry of the graphene, he switched from real NNN to imagianary. We now follow the same logic, and analyze the symmetries.

$$H = \sum_{n=1}^{N}(t+\delta t)c_n^\dagger d_n + \sum_{n=1}^{N-1}[(t-\delta t)c_{n+1}^\dagger d_n + iKc_i^\dagger c_{i+1} - iKd_i^\dagger d_{i+1} + h.c]. \quad (3.10)$$

Therefore, Bloch Hamiltonian can be written as,

$$H(k) = \begin{pmatrix} 2Ksink & t+\delta t+(t-\delta t)e^{-ik} \\ t+\delta t+(t-\delta t)e^{ik} & -2Ksink \end{pmatrix}. \quad (3.11)$$

Investigating the TRS, we see that

$$\begin{aligned} \mathbf{1}\mathcal{K}\ (2Ksink\ \sigma_z)\ \mathbf{1}\mathcal{K} &= 2Ksink\ \sigma_z \\ \Rightarrow H^*(k) &\neq H(-k) \end{aligned} \quad (3.12)$$

where for the last line, we used Eq. (2.14) with $\mathcal{U} = \mathbf{1}$. Therefore, as expected, complex hopping breaks the TRS. We can also show that, Eq. (3.11) has particle-hole symmetry. Since the model is $H_{SSH} + H_{NNN}$, and H_{SSH} has the PHS, we just need to show that, NNN term satisfies it as well. Taking the $\mathcal{C} = \sigma_z\mathcal{K}$,

$$\left.\begin{aligned} &\sigma_z\mathcal{K}\ (2Ksink\ \sigma_z)\ \mathcal{K}\sigma_z = 2Ksink\ \sigma_z \\ &(2Ksink\ \sigma_z) = -(2Ksin(-k)\ \sigma_z) \end{aligned}\right\} \Rightarrow \mathcal{C}H(k)\mathcal{C}^{-1} = -H(-k). \quad (3.13)$$

So that it holds. Since there is no TRS but PHS holds, chiral symmetry does not exist. Hence, it is class D with a topological index of $\mathbb{Z}_2$. As it pointed out before, winding number has no use as hamiltonian contains all of three pauli matrices.

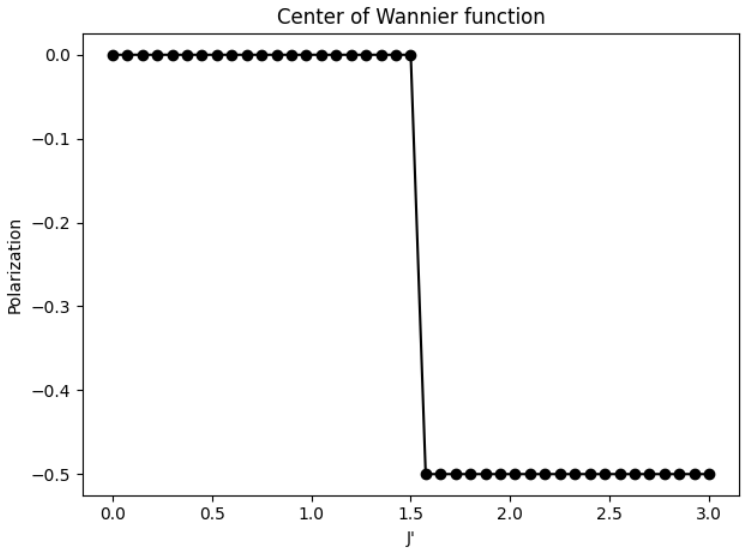

Figure 3.4: Polarization vs J' with J = 1.5, K = 1. As J'=J, the phase transition occurs and polarization jumps to -0.5

Therefore, we look at the polarization in order to differentiate between trivial and topological phases.

As it can be seen from Fig. 3.4, the phase transition occurred at $J' = 1.5$ again independent of the value of K. The graph is exact copy of the Fig. 2.7, where K value was 0. Note that, although in Fig. 2.7 the value for polarization jumps to 0.5 and -0.5 in the newly obtained one, they are equal, as we have derived in Eq. (2.49), stating that polarization values differ by an integer are equal. Therefore, we can safely conclude that, $\mathbb{Z}_2$ invariant can be calculated through the polarization, or Zak phase. However, the gauge invariant in mod m behavior of polarization gives rise a problem in $\mathbb{Z}$ topological index where SSH hamiltonian belongs, which we will show now.

3.3 Enlarged SSH Model

In this section, in order to prove that polarization value does not correspond to topological index in $\mathbb{Z}$ type of topological insulators, we enlarged the SSH model.

We take the normal SSH model and add second nearest neighbor hopping from B sublattice to A sublattice as shown in Fig. 3.5. Hence, the Bloch hamiltonian takes the form,

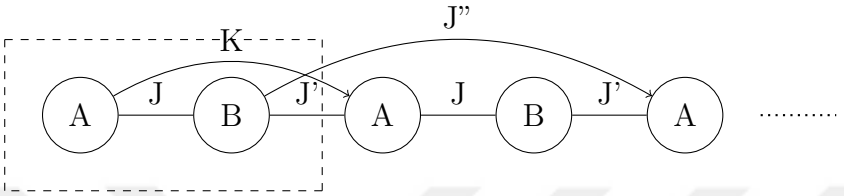

Figure 3.5: Enlarged SSH model, with added J'' hopping. K = 0 for the convenience.

$$H(k) = \begin{pmatrix} 0 & J + J'e^{-ik} + J''e^{-2ik} \\ J + J'e^{ik} + J''e^{2ik} & 0 \end{pmatrix} \tag{3.14}$$

where we denoted the extra term with J''. In order to find the gap closure points, we solve the eigenvalue equation,

$$\begin{bmatrix} 0-\lambda & J + J'e^{-ik} + J''e^{-2ik} \\ J + J'e^{ik} + J''e^{2ik} & 0-\lambda \end{bmatrix} = 0. \tag{3.15}$$

Parameterizing the Eq. (3.15) with $J = t + \delta t$, $J' = t - \delta t$ and $J'' = \Delta t$ and taking $t = 1$, we can find the gap closure values as,

$$(1+\delta)^2+(1-\delta)^2+\Delta^2+2[(1-\delta^2)cosk+\Delta(1-\delta)cosk+\Delta(1+\delta)cos2k] = 0. \tag{3.16}$$

Checking $k = 0$ case, we have,

$$\begin{aligned} 2 + 2\delta^2 + \Delta^2 + 2[1 - \delta^2 + 2\Delta] &= 0 \\ \Rightarrow 4 + \Delta^2 + 4\Delta &= 0 \\ \Rightarrow \Delta &= -2. \end{aligned} \tag{3.17}$$

Another k point to be checked is $k = \pi$

$$
\begin{aligned}
2 + 2\delta^2 + \Delta^2 + 2[\delta^2 - 1 + \Delta(\delta - 1) + \Delta(1 + \delta)] = 0 \\
\Rightarrow 4\delta^2 + \Delta^2 + 4\Delta\delta = 0 \\
\Rightarrow \Delta = 2\delta
\end{aligned}
\tag{3.18}
$$

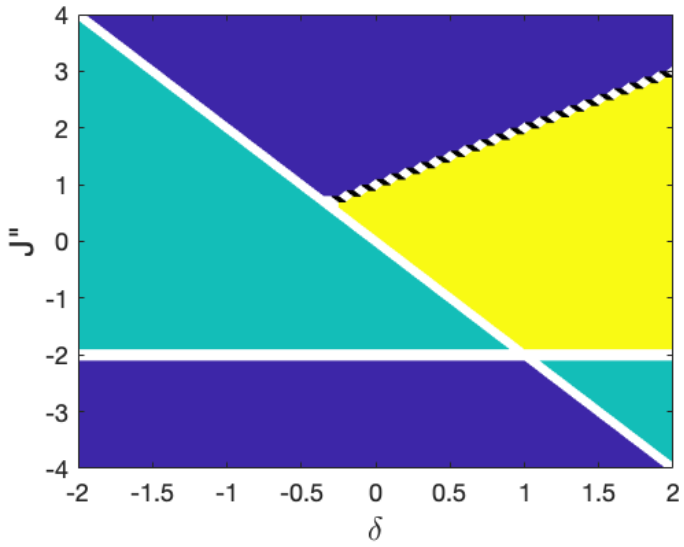

Figure 3.6: Winding number of the enlarged SSH model. Yellow region corresponds to $\nu = 0$, light blue region has $\nu = 1$ and dark blue region has $\nu = 2$ and white regions correspond to gap closure points.

Since the other root is not easy to find, we plotted the winding number as a function of J'' and δ. The two gap closure can be seen via white lines, where one of them occurred at $J'' = 2$ and the other at $J = -2\delta$. As it can be seen from Fig. 3.6, there is one other root with $J'' - \delta = 1$ with k $= \pm arccos(\delta - 1/2J'')$, which can be seen as altering white and black colors. Taking $J'' = 0$, we recover the original SSH model and phase transition occurs at $\delta = 0$. It is interesting that, ν goes from 0 to 2, without having the value of $\nu = 1$ for $\delta = 1$ with altering $J'' = 0 \rightarrow 2$. We also plot the polarization of the system for the same values in the Fig. (3.7).

Now the difference is more obvious. Since the polarization $\mathcal{P} = \gamma/2\pi$ and we can write $\gamma = \nu\pi(mod 2\pi)$, we can see that $\mathcal{P}_{Yellow} = \mathcal{P}_{DarkBlue} - 1$. Since the polarization $\mathcal{P}$ is invariant in mod m with m being an integer, yellow and dark blue regions have the same polarization as it can be seen in Fig. 3.6, whereas their

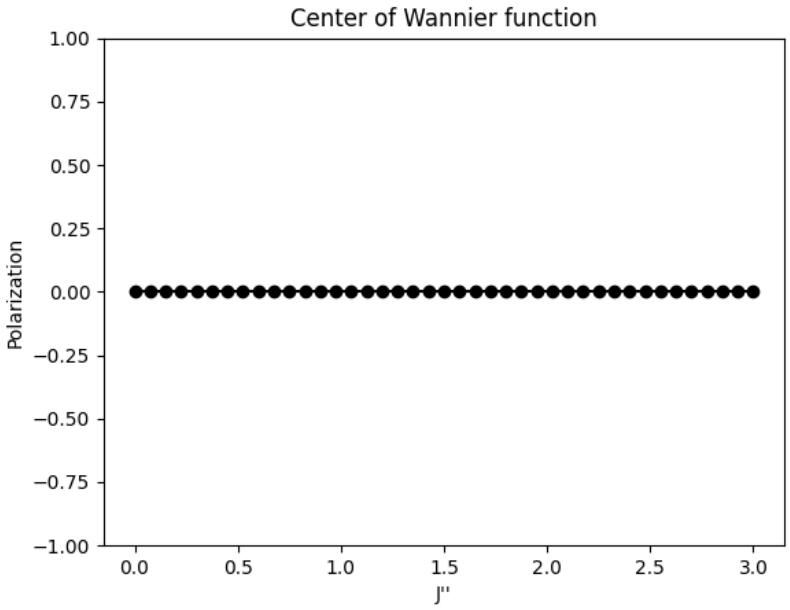

Figure 3.7: Polarization of the enlarged SSH model as J" varies from 0 to 2. We took δ to be 0.5

winding numbers are different, hence their topological properties. Therefore, we can conclude that, $\mathcal{P}_{electric}$ cannot differentiate the different topological phases where difference in the winding number is 2 and should not be used when the topological index is $\mathbb{Z}$ with d = 1.

The next interesting part to show is, how the winding number jumps from 0 to 2. Here we do this by changing the value of J''. As it can be seen from Fig. 3.8 that, at $J'' = 1.5$, the inner and outer circle touches the origin. Hence, when $J'' > 1.5$, they both wind the origin, making $\nu = 2$. This is exactly what happens at Fig. 3.6, when $\nu = 0$ to $\nu = 2$ transition occurs, which is the transition from yellow to dark blue region. The change in the winding number from 0 to 2 can be seen from Fig. 3.8.

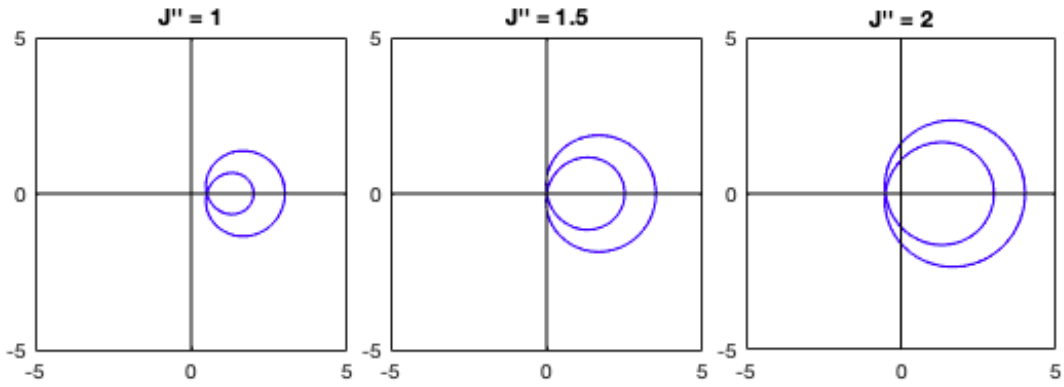

Figure 3.8: Graphical winding number of the enlarged SSH model. Changing $\nu = 0$ to $\nu = 2$ is shown for $\delta = 0.5$

Chapter 4

SSH Model with Distance Dependence

Through the discussion, the distance between A and B sublattice has been ignored such that in tight binding model, we took orbitals as if they are on top of each other. In this chapter, we investigate the distance dependent SSH model [22].

4.1 Complex Hopping with Distance Dependence

As in the previous chapter, we take a next-nearest neighbor with complex hopping amplitude such that it breaks time-reversal symmetry. We now assume that, the distance between A and B sublattice is p/q with p and q are being co-primes. Hence, the Bloch Hamiltonian takes the form,

$$\begin{pmatrix} 2Ksink & J\exp(ikp/q) + J'\exp(-ik(1-p/q)) \\ J\exp(-ikp/q) + J'\exp(ik(1-p/q)) & -2Ksink \end{pmatrix}. \tag{4.1}$$

Using Pauli matrices, we can write,

$$\begin{aligned}\tilde{d_x} &= J\cos(kp/q) + J'\cos(k(1-p/q)) \\ \tilde{d_y} &= -J\sin(kp/q) + J'\sin(k(1-p/q)) \\ \tilde{d_z} &= 2K\sin k.\end{aligned} \tag{4.2}$$

In an open form, we can write $\tilde{dx}$ and $\tilde{dy}$ as,

$$\begin{aligned}\tilde{d_x} &= J\cos(kp/q) + J'\cos k\ \cos(kp/q) + J'\sin k\ \sin(kp/q) \\ \tilde{d_y} &= -J\sin(kp/q) + J'\sin k\ \cos(kp/q) - J'\cos k\ \sin(kp/q).\end{aligned} \tag{4.3}$$

Therefore, we can connect SSH model without distance dependence, which we denote as d_x and d_y, to SSH model with distance dependence, denoted as $\tilde{d_x}$ and $\tilde{d_y}$. Hence, we can write,

$$\begin{bmatrix}\tilde{d_x} \\ \tilde{d_y}\end{bmatrix} = \begin{bmatrix} cos(k(p/q)) & sin(k(p/q)) \\ -sin(k(p/q)) & cos(k(p/q))\end{bmatrix}\begin{bmatrix}d_x \\ d_y\end{bmatrix}. \tag{4.4}$$

As it can be seen, distance dependent and independent models are connected via rotation about the z-axis. Although the rotation in z-axis is applied, distance dependent Bloch Hamiltonian still has the same symmetries. Particle-hole symmetry remains in the system with $\mathcal{C} = \sigma_z\mathbf{K}$. Since there are no other symmetries, distance dependent SSH model is classified by $\mathbb{Z}_2$ label.

When the system is labeled by $\mathbb{Z}_2$ index, the topologically distinct states cannot be found by winding number. However, the interesting behaviour of the three dimensional d_x, d_y and d_z plot can be seen in Fig. 4.1.

When the Brillouin zone is not extended for the case for $p/q = 1/2$, the curve traced by parameter $d(k)$ is left open. However, due to the fact that the system is periodic, the end point should be connected to starting point. In order to gain insight why it should be extended, we can look at the problem of electron in a box. Assume that the electron in a one dimensional system with Born-von Karman boundary conditions such that, $\Psi(x) = \Psi(x + L)$. Using the ordinary approach, in order to calculate the position expectation of the electron, we can write,

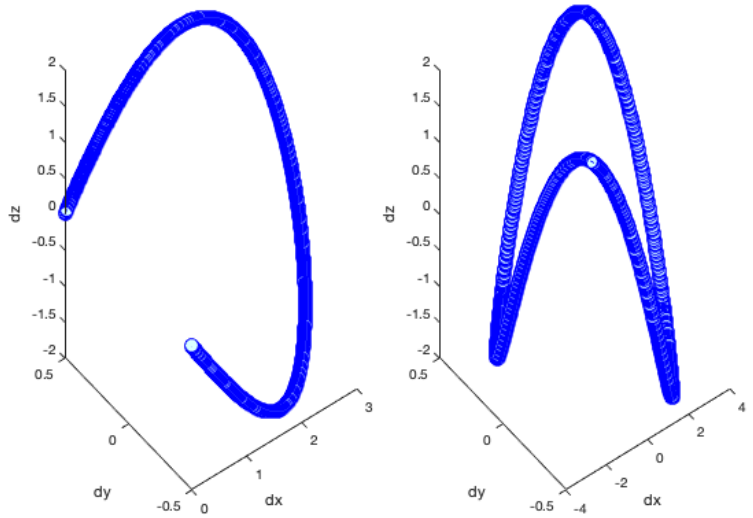

Figure 4.1: Two different curves, traced by the d_x, d_y and d_z with $p/q = 1/2$. First figure belongs to $k \in [-\pi, \pi]$. The second figure has $k \in [-2\pi, 2\pi]$

$$\langle x \rangle = \int dx x \left|\Psi(x)\right|^2 . \tag{4.5}$$

However, due to the BvK, the expectation value is ill-defined, so is the polarization of the system. Therefore, Resta [10] provided a new definition to evaluate the expectation value as,

$$\begin{aligned} z &= \langle \Psi | \, e^{i(2\pi/L)x} \, |\Psi\rangle \\ \Rightarrow \langle x \rangle &= \frac{L}{2\pi} \mathrm{Im} \log z \end{aligned} \tag{4.6}$$

where z is in general a complex number. Therefore, the polarization can be expressed as,

$$\mathcal{P} = \frac{e}{2\pi} \mathrm{Im} \log z. \tag{4.7}$$

Assuming a non-degenerate ground state Ψ, we take a $\mathbf{T}$ operator such that, acting on the Ψ, we have $\mathbf{T}\Psi = \exp(iK)\Psi$, such that $\mathbf{T}$ operator translates a unity to the right. We can squeeze z operator described in the Eq. (4.6) between $\mathbf{T}$ operators.

$$\mathbf{T}e^{i(2\pi/L)\hat{x}}\mathbf{T}^{\dagger} = e^{2i\pi n_0}e^{i(2\pi/L)\hat{x}}. \tag{4.8}$$

Then we can write the following argument,

$$\begin{aligned}
\langle\Psi|\, e^{i(2\pi/L)\hat{x}}\,|\Psi\rangle &= \langle\Psi|\, \mathbf{T}^{\dagger}\mathbf{T}e^{i(2\pi/L)\hat{x}}\mathbf{T}^{\dagger}\mathbf{T}\,|\Psi\rangle \\
&= \langle\Psi|\, \mathbf{T}^{\dagger}e^{2i\pi n_0}e^{i(2\pi/L)\hat{x}}\mathbf{T}\,|\Psi\rangle \\
&= \langle\Psi|\, e^{-iK}e^{2i\pi n_0}e^{i(2\pi/L)\hat{x}}e^{iK}\,|\Psi\rangle \\
&= e^{2i\pi n_0}\,\langle\Psi|\, e^{i(2\pi/L)\hat{x}}\,|\Psi\rangle\,.
\end{aligned} \tag{4.9}$$

Therefore, if n_0 is not an integer, Eq. (4.6) becomes zero. Since the argument is restrictive, Aligia and Ortiz [23] considered the operator such that, for any arbitrary fillings of the form $n_0 = n/l$, the new operator to calculate the expectation value of the position, z , becomes

$$z[n/l] = \langle\Psi|\, e^{i(\frac{2\pi}{L})l\hat{x}}\,|\Psi\rangle\,. \tag{4.10}$$

As it can be seen from Eq. (4.10) that, the exponential is multiplied by l in order to not get zeros when n_0 is not an integer. Same reasoning applies to our case, where, if the distance between the sublattices are not integers but fractions, Eq. (4.10) is needed instead of usual definition of Eq. (4.6). Extending the BZ by q times as in the Fig. 4.1, we end up with a curve which is closed, as expected.

Taking $p/q = 1/3$, we plot the curves traced out by d_x, d_y and d_z in two dimensions. The left figure is unknot, whereas the right figure is trefoil knot.[1] The middle figure corresponds to gap closure. We now introduce the Reidemeister moves in order to show that, the left figure is actually unknot.

[1]Since the plots are normally in 3d, in order to understand which line is above or below, the erased line is below from the plotted line.

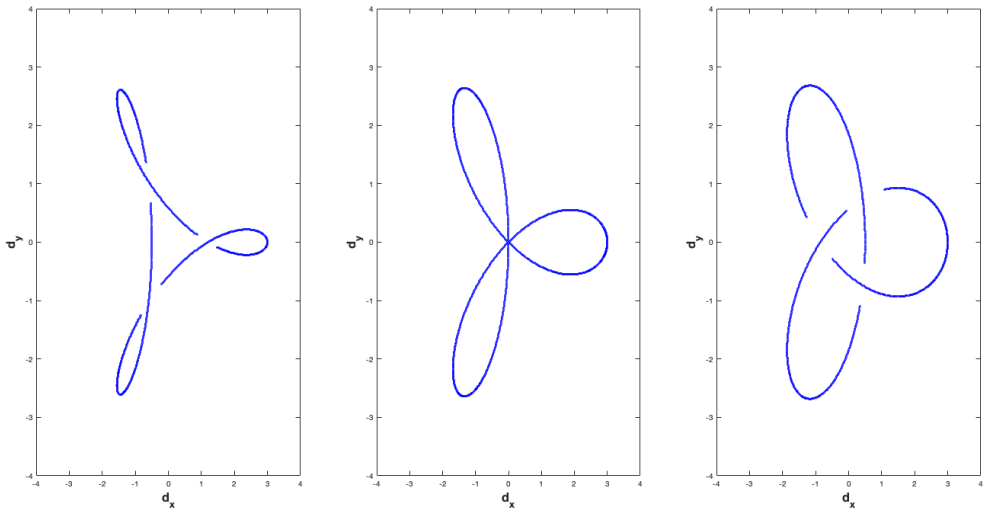

Figure 4.2: Curves traced out by d_x, d_y and d_z. The left figure has $J = 1.75, J' = 1.25$. Middle figure has $J = 1.5, J' = 1.5$, and the right figure has $J = 1.25, J' = 1.75$

4.1.1 Reidemeister Moves

In knot theory, in order to distinguish unknot from the knot, a German mathematician Kurt Reidemeister introduced three moves where the topology of the knot is unchanged. So the theorem basically states that, two shapes or diagrams are equal if they can be deformed into each other via three possible moves.

R1 is a move such that, it either adds or removes a twist from the knot. R2 applies when one of the curve is above the other such that, applying the move, we either remove or add two crossings above or below. R3 is called slide such that, a strand can be slid from one side to the other with crossing. Looking at the left plot of the Fig. 4.2, it can be seen that, applying R1 move to all twists, it becomes unknot. Therefore left figure and unknot has the same topology. Looking at the right figure, however, the crossings cannot be removed by any Reidemeister moves. Therefore, right figure is called trefoil knot in the knot theory and has different topological properties than unknot. So, we can conclude that, when $J = J'$, the phase transition occurs and the transition is realized without looking at the polarization which is the main quantity to look at when the index is $\mathbb{Z}_2$.

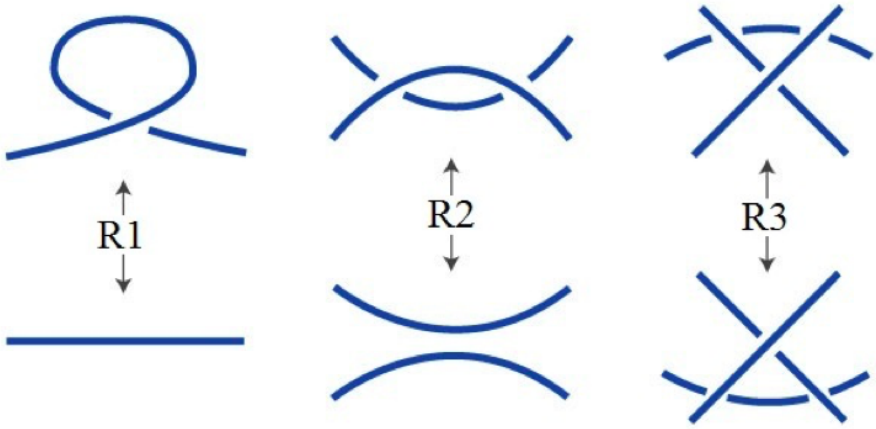

Figure 4.3: Three Reidemeister moves, adopted from [4]

.

However, not all the co-primes of p and q give knot distinction as we pass the gap closure points. We show this at Fig. 4.4.

As it can be seen, topologically distinct states, left and right figures are both unknots. Therefore for the $p/q = 1/2$ case, knot behaviour couldn't distinguish the different phases of the Hamiltonian.[2] The reason for this behavior is that, the most simplistic unknot is trefoil knot as we have shown in Fig. 4.3 and the rotation around the body of the trefoil itself is three. So, in order to get knotted behavior for the topologically non-trivial state, BZ must be enlarged at least three times.

We give the polarization of the $p/q = 1/3$ and the $p/q = 1/2$ case in Fig. 4.5, where the polarization value is changed with respect to the SSH model where the sublattices are on top of each other.

Comparing Fig 4.5 with the Fig. 3.4, where distance dependence is ignored, the polarization values are shifted by $\frac{1}{2}(\frac{p}{q})$. Since q is the number that specifies the rotation around the body of the knot, it is suspicious that, there might be an easier way to calculate the polarization.

[2]However, polarization still can distinguish the different topological phases for $p/q = 1/2$ case.

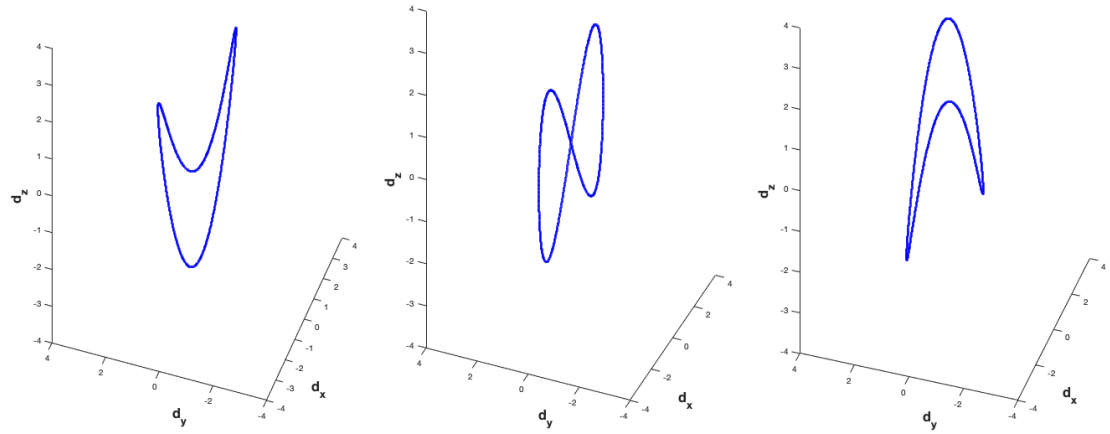

Figure 4.4: Curves traced out by d_x, d_y and d_z with p/q = 1/2. The left figure has $J = 1.75, J' = 1.25$. Middle figure has $J = 1.5, J' = 1.5$, and the right figure has $J = 1.25, J' = 1.75$

As it is discussed before, 2×2 systems with d_z entry, the winding number is useless to differentiate between different topological states since the $d(k)$ is a three dimensional vector. However, when knots are formed, winding number gives the topological behaviour or the polarization. As we mentioned q is being the number of rotations around the body, which we call w_2, and the ordinary winding number, number of loops around the origin, w_1, so the polarization value of the system is given by,

$$\mathcal{P} = \frac{e}{2}\frac{w_1}{w_2}. \tag{4.11}$$

Eq. (4.11) can also be justified by using the inversion symmetry of the form Eq. (3.6). As Eq. (4.1) still satiesfies the inversion symmetry, we can use the Wilson loop approach. For the distance of p/q between A and B sublattice of the unit cell, the inversion center can be found at $p/2q$ and the other inversion center is located at $(p+q)/2q$. The wannier centers of the SSH model shift from $w(x) = \pm w(-x), w(-x+a) = \pm w(x)$ to $w(x) = \pm w(-x+p/q), w(-x+1+p/q) = w(x)$,

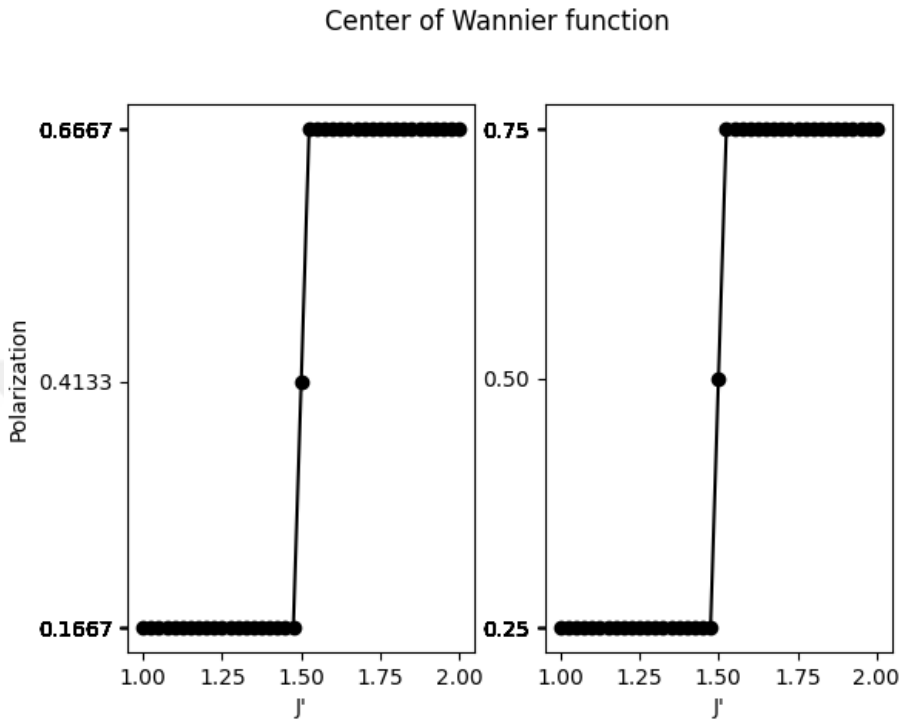

Figure 4.5: Polarization values for different co-primes. Left figure is for $p/q = 1/3$ and right figure is for $p/q = 1/2$. For all calculations, $J = 1.5$ and $K = 1$ is used.

so that the wannier states are located at either $x = p/2q$ or $x = (q + p)/2q$. For example, taking a case of $p/q = 1/3$, the polarization values can take $1/6$ or $2/3$ as in the case of Fig. 4.5.

Looking at the Fig. 4.2, left figure has $w_1 = 1$ and $w_2 = 3$ as both of them are formed clockwise. For the right figure, while $w_1 = 2$ is formed in clockwise, $w_2 = 3$ is formed anti-clockwise. Taking $e = 1$, then $\mathcal{P} = 1/6$ for the left figure and $\mathcal{P} = -2/3$ for the right figure. Since the polarization is invariant in mod m with m is being an integer, $\mathcal{P} = -2/3 \overset{\text{mod1}}{=} 1/3$. As it can be seen, they match with what has been found in Fig. 4.5.

From the discussion, $J = J'$ at $k = \pm\pi$ is the gap closure point. So the phase transition is occurs at these points, independent of the value of K. However, knots are affected by the change of the value of p/q. Here we also investigate what happens when $p/q = 2/3$ instead of $1/3$. From the inversion symmetry, which has

the form $\sigma_x H(k)\sigma_x = H(-k)$, it can be guessed that, changing $p/q = 1/3 \to 2/3$, would change $A \to B$ and $B \to A$. Therefore, we now expect that, trefoil knot occurs when $J > J'$, total opposite of the Fig. 4.2 where the knot is formed when $J' > J$, which can be seen in Fig 4.6.

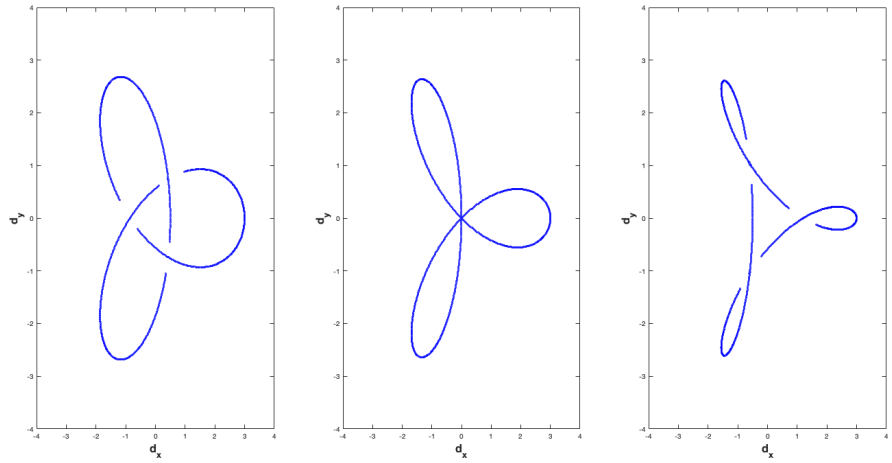

Figure 4.6: Curves traced out by d_x, d_y and d_z with p/q = 2/3. The left figure has $J = 1.75, J' = 1.25$. Middle figure has $J = 1.5, J' = 1.5$, and the right figure has $J = 1.25, J' = 1.75$

Chapter 5

SSH model with Spin-Orbit Coupling

Through the discussion, we always neglected the spin of the electron, making the system spinless. In this chapter, we follow the Kene-Mele hamiltonian, introducing the spin-orbit coupling and Rashba term.

Taking the Eq. (3.11), we first add spin to the system, making the Bloch Hamiltonian a 4×4 matrix. There are two ways of making the system spinful. The simple one is, for the chrial symmetry breaking term, we can double it such that, in the spinful system, it has the form of $2Ksink\ \mathbb{1} \otimes \sigma_z$. However, this is just a 2 SSH model, separated by spins. Considering the Haldene Hamiltonian, the more interesting one has the form $\sigma_z \otimes \sigma_z$ in which the Dirac fermions has opposite masses. Therefore, newly obtained one can be written as[1] [2]

$$H(k) = (J + J'cosk)\mathbb{1} \otimes \sigma_x + J'sink\ \mathbb{1} \otimes \sigma_y + 2Ksink\ \sigma_z \otimes \sigma_z. \tag{5.1}$$

[1]Here we use the following basis: $(a^\dagger_{n\uparrow} b^\dagger_{n\uparrow} a^\dagger_{n\downarrow} b^\dagger_{n\downarrow})\ H(k)(a_{n\uparrow} b_{n\uparrow} a_{n\downarrow} b_{n\downarrow})^T$

[2]Dirac fermions with opposite masses in the real space reads,

$$H = iK \sum a^\dagger_{n\uparrow} a_{n+1\uparrow} - iK \sum b^\dagger_{n\uparrow} b_{n+1\uparrow} - iK \sum a^\dagger_{n\downarrow} a_{n+1\downarrow} iK \sum b^\dagger_{n\downarrow} b_{n+1\downarrow} + h.c$$

As it has been discussed in the chapter 3, where introducing the complex hopping breaks the time-reversal symmetry, one can expect that, it also breaks the TRS here. However, due to the $\mathcal{T}$ opeartor behaves differently for the spin-1/2 systems, as we will show, this is not the case.

In the most general form, we have $\mathcal{T} = \mathcal{U}\mathcal{K}$, with $\mathcal{U}$ is being a unitary matrix. Therefore, squaring the $\mathcal{T}$,

$$\begin{aligned} \mathcal{T}^2 &= \mathcal{U}\mathcal{K}\mathcal{U}\mathcal{K} \\ &= \mathcal{U}\mathcal{U}^* \\ &= \mathcal{U}(\mathcal{U}^T)^{-1} \\ &= \phi \end{aligned} \tag{5.2}$$

where we used the fact that $\mathcal{U}\mathcal{U}^\dagger = \mathbb{1}$ from going second equality to third equality. The last line may come as a surprise but, using a unitary operator such as σ_y, it can be shown that $\sigma_y\sigma_y^* = -\mathbb{1}$.

Using Eq. (5.2), we can write $\mathcal{U} = \phi\mathcal{U}^T$ and transposing both sides, we have $\mathcal{U}^T = \mathcal{U}\phi$. Hence,

$$\mathcal{U} = \phi\mathcal{U}\phi \tag{5.3}$$

we proved that Eq. (5.3) holds only for $\phi = \pm 1$. For spinless(spinful) particles, like in SSH model, $\phi = 1(\phi = -1)$. Therefore, doubling the system with spin as in Eq. (5.1), we now show that TRS holds although the system is similar to what has been investigated in chapter 3. We now show that Eq. (5.1) satisfies $\mathcal{T}H(k)\mathcal{T}^{-1} = H(-k)$ with $\mathcal{T}$ is taken as $\mathcal{T} = -i(\sigma_y \otimes \mathbb{1})\mathcal{K}$.[3]

$$\begin{aligned} &- i(\sigma_y \otimes \mathbb{1})\mathcal{K}(\mathbb{1} \otimes \sigma_x)i(\sigma_y \otimes \mathbb{1})\mathcal{K} \\ &- i(\sigma_y \otimes \mathbb{1})\mathcal{K}(\mathbb{1} \otimes \sigma_x)(-i(\sigma_y^* \otimes \mathbb{1})) \\ &- (\sigma_y \otimes \mathbb{1})\mathcal{K}(\mathbb{1} \otimes \sigma_x)(\sigma_y^* \otimes \mathbb{1}) \\ &= \mathbb{1} \otimes \sigma_x \end{aligned} \tag{5.4a}$$

[3]Using $\mathcal{T}^2 = -1$, $\mathcal{T} = -\mathcal{T}^{-1}$

$$
\begin{aligned}
&- i(\sigma_y \otimes \mathbb{1})\mathcal{K}(\mathbb{1} \otimes \sigma_y)i(\sigma_y \otimes \mathbb{1})\mathcal{K} \\
&- i(\sigma_y \otimes \mathbb{1})\mathcal{K}(\mathbb{1} \otimes \sigma_y^*)(-i(\sigma_y^* \otimes \mathbb{1})) \\
&= -\sigma_y \otimes \mathbb{1}
\end{aligned} \tag{5.4b}
$$

$$
\begin{aligned}
&- i(\sigma_y \otimes \mathbb{1})\mathcal{K}(\sigma_z \otimes \sigma_z)i(\sigma_y \otimes \mathbb{1})\mathcal{K} \\
&- i(\sigma_y \otimes \mathbb{1})\mathcal{K}(\sigma_z \otimes \sigma_z)(-i(\sigma_y^* \otimes \mathbb{1})) \\
&= -\sigma_z \otimes \sigma_z
\end{aligned} \tag{5.4c}
$$

which confirms $-i(\sigma_y \otimes \mathbb{1})$ as the time-reversal operator since cosine is an even and sine is an odd function. The lengthy calculations will not be shown here for other operators. For other symmetries, we introduce the gamma matrices as $\Gamma_{1,2,3,4,5} = (\mathbb{1}\otimes\sigma_x), (\mathbb{1}\otimes\sigma_z), (\sigma_x\otimes\sigma_y), (\sigma_y\otimes\sigma_y), (\sigma_z\otimes\sigma_y)$. The remaining matrices can be found from the generator of Dirac algebra, $\Gamma_{ab} = [\Gamma_a, \Gamma_b]/2i$. Therefore, the Hamiltonian in Eq. (5.1) can be written as,

$$
H(k) = d_1\Gamma_1 - d_{12}\Gamma_{12} + d_{15}\Gamma_{15} \tag{5.5}
$$

with $d_1 = J + J'cosk, d_{23} = J'sink$ and $d_{15} = 2Ksink$. Using the fact that $\mathcal{T}H(k)\mathcal{T}^{-1} = H(-k)$, we can see that, matrices that has the form of $\left\{\Gamma_a, \Gamma_b\right\} = 2\delta_{ab}$ transform as $d_{ab}(k) = -d_{ab}(-k)$. Other generators of the Dirac algebra, however, has the form of $d_a(k) = d_a(-k)$.

For partice-hole symmetry, $\mathcal{C}H(k)\mathcal{C}^{-1} = -H(-k)$ has to be satisfied. Using $\mathcal{C} = (\sigma_z \otimes \sigma_z)\mathcal{K}$, it can be shown that,

$$
\mathcal{C}\Gamma_1\mathcal{C}^{-1} = -\Gamma_1 \tag{5.6a}
$$

$$
\mathcal{C}\Gamma_{12}\mathcal{C}^{-1} = \Gamma_{12} \tag{5.6b}
$$

$$
\mathcal{C}\Gamma_{15}\mathcal{C}^{-1} = \Gamma_{15} \tag{5.6c}
$$

As cosine is an even and sine is an odd function, Eq. (5.6) also holds.

Trying out chiral symmetry operator is not necessary as both $\mathcal{T}$ and $\mathcal{C}$ exist. As it is shown in the chapter 2, chiral symmetry operator $\mathcal{S}$ can be found from the multiplication of the operators. Therefore,

$$\begin{aligned}\mathcal{S} &= \mathcal{T}\mathcal{C} \\ &= -i(\sigma_y \otimes \mathbb{1})\mathcal{K}\ (\sigma_z \otimes \sigma_z)\mathcal{K} \\ &= \sigma_x \otimes \sigma_z\end{aligned} \tag{5.7}$$

Using the operators, we can square them and look for the topological invariant. Since $\mathcal{T}^2 = -1$, $\mathcal{C}^2 = 1$ and $\mathcal{S}^2 = 1$, in one dimension, the model has the $\mathbb{Z}_2$ topological invariant and hence, it is classified by the polarization of the system. However, the model as present, is not very interesting since it is 2 SSH model which can be diagonalized and can be found that, it is degenerate everywhere since it is not spin-split and gives the exact same properties of SSH model with complex hopping amplitude. Thus, in order to separate the degenerate bands, we also introduce the Rashba spin-orbit coupling as,

$$H_{rashba} = i\lambda_r \sum_{n=1}^{N} a^\dagger_{n\uparrow} b_{n\downarrow} + a^\dagger_{n\downarrow} b_{n\uparrow} + i\lambda_r \sum_{m=1}^{N-1} a^\dagger_{n+1\uparrow} b_{n\downarrow} + a^\dagger_{n+1\downarrow} b_{n\uparrow} + h.c. \tag{5.8}$$

Fourier transforming Eq. (5.8),

$$H_{rashba}(k) = i\lambda_r \sum_k [a^\dagger_{k\uparrow} b_{k\downarrow}(1+e^{ik}) - b^\dagger_{k\downarrow} a_{k\uparrow}(1+e^{-ik}) + a^\dagger_{k\downarrow} b_{k\uparrow}(1+e^{ik}) - b^\dagger_{k\uparrow} a_{k\downarrow}(1+e^{-ik})]. \tag{5.9}$$

In terms of gamma matrices, we can write Eq. (5.9) as,

$$H_{rashba}(k) = -\lambda_r \sum_k [(1 + cosk)\sigma_x \otimes \sigma_y + (sink)\sigma_x \otimes \sigma_x]. \tag{5.10}$$

Now it can be checked whether rashba spin-orbit coupling obeys the TRS and PHS or not. As $\sigma_x \otimes \sigma_y$ is one of the gamma matrices, it must transform as $d_3(k) = d_3(-k)$ under TRS and since cosine is an even function, it is satisfied. The same logic can be applied to other term where $\sigma_x \otimes \sigma_x$ is not one of the gamma matrices, therefore must transform as $d_3(k) = -d_3(-k)$ and oddness of the sine function satisfies it. Therefore, we can conclude that newly added term to hamiltonian obeys the TRS. The same procedure can be applied to PHS operator which reads,

$$
\begin{aligned}
&(\sigma_z \otimes \sigma_z)(\sigma_x \otimes \sigma_x)(\sigma_z \otimes \sigma_z) \\
&= \sigma_x \otimes \sigma_x
\end{aligned}
\tag{5.11a}
$$

$$
\begin{aligned}
&(\sigma_z \otimes \sigma_z)(\sigma_x \otimes \sigma_y^*)(\sigma_z \otimes \sigma_z) \\
&= -\sigma_x \otimes \sigma_y
\end{aligned}
\tag{5.11b}
$$

which obeys to $\mathcal{C}H(k)\mathcal{C}^{-1} = -H(-k)$.

Looking at the Fig. (2.4), it can be concluded that the system is in class DIII with the topological index of $\mathbb{Z}_2$. However, this time, finding the index is difficult as the Hamiltonian is a 4×4 matrix, and degenerate at the TRIM. In order to see the degeneracy, we need to discuss Kramers' Theorem.

5.0.1 Kramers' Theorem

For a TR-invariant system like we investigate, when $\mathcal{T}^2 = -1$, the system is at least two-fold degenerate. We can prove this using the fact that, for TR-invariant systems, $[H, \mathcal{T}] = 0$. Hence, if the $|\psi\rangle$ is a single particle eigenstate with energy E, the state $\mathcal{T}|\psi\rangle$, should also be an energy eigenstate with an energy E. Now assume the contrary such that, $|\psi\rangle$ and $\mathcal{T}|\psi\rangle$ only differs by a phase $\mathcal{T}|\psi\rangle = e^{i\theta}|\psi\rangle$. Multiplying by $\mathcal{T}$, we have

$$
\begin{aligned}
&\mathcal{T}^2|\psi\rangle = \mathcal{T}e^{i\theta}|\psi\rangle = e^{-i\theta}\mathcal{T}|\psi\rangle \\
&\Rightarrow -|\psi\rangle = e^{-i\theta}e^{i\theta}|\psi\rangle \\
&-|\psi\rangle = |\psi\rangle\,.
\end{aligned}
\tag{5.12}
$$

As it can be seen that, the assumption is incorrect, therefore, $|\psi\rangle$ and $\mathcal{T}|\psi\rangle$ are orthogonal to each other. At TRIM, then, we have at least double degeneracy. This can also be seen from Fig. 5.1, TRIM points have degeneracies, therefore, non-Abelian Berry connection must be used in order to find the topological invariant.

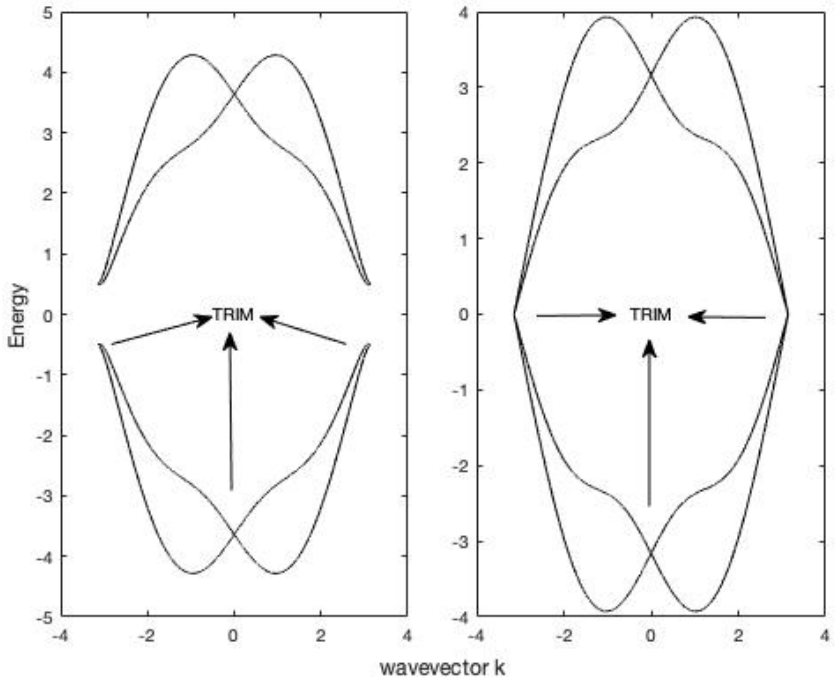

Figure 5.1: Left figure for $J = 2$, $J' = 1.5$, $K = 1$, $\lambda_r = 0.5$, right figure for $J = 1.5$, $J' = 1.5$, $K = 1$, $\lambda_r = 0.5$. Gap closure occurs at $k = \pm\pi$

5.1 Time-Reversal Polarization

Through the discussion, we calculated the charge polarization in terms of Berry connection, integrated over the 1st Brillouin zone. However, due to the Kramers' theorem, we deduced that energy values comes in pairs. Hence, instaed of calculating the connection over the whole Brillouin zone, we can compute the same properties using the Kramers' pairs using only the half the BZ.

Denoting the Kramers' pairs with the I and II, because of the time-reversal symmetry, we can relate the eigenstates of positive k of band I with the eigenstates of negative k of band II as,

$$
\begin{aligned}
|u^I_{-k,a}\rangle &= e^{i\theta(k,a)}\mathcal{T}\,|u^{II}_{k,a}\rangle \\
\mathcal{T}\,|u^I_{-k,a}\rangle &= -e^{-i\theta(k,a)}\,|u^{II}_{k,a}\rangle \\
|u^{II}_{k,a}\rangle &= -e^{i\theta(k,a)}\mathcal{T}\,|u^I_{-k,a}\rangle \\
\Rightarrow |u^{II}_{-k,a}\rangle &= -e^{i\theta(-k,a)}\mathcal{T}\,|u^I_{k,a}\rangle\,.
\end{aligned}
\tag{5.13}
$$

Using the above strategy, using only one Kramers' pair of the full Brillouin zone, we can write the polarization as,

$$
P^{I,II} = \frac{1}{2\pi}\int_{-\pi}^{\pi} A^{I,II}(k)dk \tag{5.14}
$$

where $A^{I,II}(k)$ is the Berry connection. In order to write in terms of the half Brillouin zone, we need to use two of the Kramers' pairs.

$$
P^I = \frac{1}{2\pi}\int_{0}^{\pi} A^I(k) + A^I(-k)dk. \tag{5.15}
$$

Since $A(k) = i\,\langle u_k|\,\nabla_k\,|u_k\rangle$, we can write $A(-k)$ as,

$$
\begin{aligned}
A^I(-k) &= i\sum_a \langle u^I_{-k,a}|\,\nabla_{-k}\,|u^I_{-k,a}\rangle \\
&= -i\sum_a \langle u^I_{-k,a}|\,\nabla_k\,|u^I_{-k,a}\rangle
\end{aligned}
\tag{5.16}
$$

Using the Eq. (5.13), we can write Eq. (5.16) as,

$$
\begin{aligned}
A^I(-k) &= -i\sum_a \langle \mathcal{T}u^{II}_{k,a}|\,e^{-i\theta(k,a)}\nabla_k e^{i\theta(k,a)}\mathcal{T}\,|u^{II}_{k,a}\rangle \\
&= -i\sum_a \langle \mathcal{T}u^{II}_{k,a}|\,\nabla_k\mathcal{T}\,|u^{II}_{k,a}\rangle - i\sum_a i\nabla_k\theta(k,a)\,\langle \mathcal{T}u^{II}_{k,a}|\,\mathcal{T}\,|u^{II}_{k,a}\rangle \\
&= -i\sum_a \langle \mathcal{T}u^{II}_{k,a}|\,\nabla_k\mathcal{T}\,|u^{II}_{k,a}\rangle + \sum_a \nabla_k\theta(k,a)
\end{aligned}
\tag{5.17}
$$

where a denotes the non-Kramers' pairs. We know need to simplify the first summation of the Eq. (5.17). Before that, we can easily prove that Berry connection is real.

$$
\begin{aligned}
A(k) &= i \langle u_k | \nabla_k | u_k \rangle \\
&= i\nabla_k(\langle u(k)|u(k)\rangle) - \langle \nabla_k u(k)|u(k)\rangle \\
&\Rightarrow \langle u_k | \nabla_k | u_k \rangle = - \langle \nabla_k u(k)|u(k)\rangle
\end{aligned}
\tag{5.18}
$$

which proves that $\langle u_k | \nabla_k | u_k \rangle$ is imaginary. Returning the Eq. (5.17), the term $\sum_a \langle \mathcal{T} u^{II}_{k,a} | \nabla_k | \mathcal{T} u^{II}_{k,a} \rangle$ should also be imaginary. Using the fact that $\mathcal{T}$ contains a unitary matrix U and complex conjugation $\mathcal{K}$, we can write this term as,

$$
\begin{aligned}
\langle \mathcal{T} u^{II}_{k,a} | \nabla_k \mathcal{T} | u^{II}_{k,a} \rangle &= u^{II}_{k,a} \nabla_k u^{II*}_{k,a} \\
&\overset{Eq.(5.18)}{=} -u^{II*}_{k,a} \nabla_k u^{II}_{k,a} \\
&= - \langle u^{II}_{k,a} | \nabla_k | u^{II}_{k,a} \rangle .
\end{aligned}
\tag{5.19}
$$

Hence, Eq. (5.17) can be written as

$$
\begin{aligned}
A^I(-k) &= i \sum_a \langle u^{II}_{k,a} | \nabla_k | u^{II}_{k,a} \rangle + \sum_a \nabla_k \theta(k,a) \\
&= A^{II}(k) + \sum_a \nabla_k \theta(k,a).
\end{aligned}
\tag{5.20}
$$

Therefore, Eq. (5.15) becomes

$$
\begin{aligned}
P^I &= \frac{1}{2\pi} \int_0^\pi A^I(k) + A^{II}(k) + \sum_a \nabla_k \theta(k,a) \\
&= \frac{1}{2\pi} \int_0^\pi A(k) dk + \sum_a \theta(\pi,a) - \theta(0,a)
\end{aligned}
\tag{5.21}
$$

where the last term is called sewing matrix and can be defined as

$$
B_{mn}(k) = \langle u_{-k,m} | \mathcal{T} | u_{k,n} \rangle . \tag{5.22}
$$

Hence, using Eq. (5.13), we can write

$$
\begin{aligned}
B^{11}_{mn}(k) &= \langle u^{I}_{-k,m}| \mathcal{T} |u^{I}_{k,n}\rangle \\
&= \langle u^{I}_{-k,m}| - e^{-i\theta(-k,n)} |u^{II}_{-k,n}\rangle \\
&= 0
\end{aligned}
\tag{5.23a}
$$

$$
\begin{aligned}
B^{21}_{mn}(k) &= \langle u^{II}_{-k,m}| - e^{-i\theta(-k,n)} |u^{I}_{-k,n}\rangle \\
&= -e^{-i\theta(-k,n)}\delta_{mn}
\end{aligned}
\tag{5.23b}
$$

$$
\begin{aligned}
B^{22}_{mn}(k) &= \langle u^{II}_{-k,m}| \mathcal{T} |u^{II}_{k,n}\rangle \\
&= \langle u^{II}_{-k,m}| e^{-i\theta(k,n)} |u^{I}_{-k,n}\rangle \\
&= 0
\end{aligned}
\tag{5.23c}
$$

$$
\begin{aligned}
B^{12}_{mn}(k) &= \langle u^{I}_{-k,m}| \mathcal{T} |u^{II}_{k,n}\rangle \\
&= \langle u^{I}_{-k,m}| e^{-i\theta(k,n)} |u^{I}_{-k,n}\rangle \\
&= e^{-i\theta(k,n)}\delta_{mn}
\end{aligned}
\tag{5.23d}
$$

As it can be seen that, sewing matrix couples only the Kramers' pairs.

$$
B = \begin{bmatrix} 0 & -e^{-i\theta(-k,n)} \\ e^{-i\theta(k,n)} & 0 \end{bmatrix} \tag{5.24}
$$

and Eq. (5.24) is anti-symmetric, like Pfaffian matrix, but only at $k = 0, \pi$.

Here, we can write Eq. (5.21) with using the sewing matrix as,

$$
P^{I} = \frac{1}{2\pi}\int_{0}^{\pi} A(k)dk + i\ log\left[\frac{Pf[B(\pi)]}{Pf[B(0)]}\right] \tag{5.25}
$$

where Pf dones for Pfaffian and the Pfaffian choses the B_{12} component of the sewing matrix. As it has been discussed in the thesis, polarization is a good choice to calculate $\mathbb{Z}_2$ invariant. As Ref. [11] showed that, Eq. (5.25) is gauge invariant, however, for a numerical calculation, an arbitrary gauge must be fixed. Instead of using Bloch wavefunctions and fixing a gauge, Ref. [24] proposed a new method to calculate Eq. (5.25) using Kato propagator which uses projection operators instead of Bloch wavefunctions, therefore, it is gauge invariant.

5.1.1 Adiabatic Theorem and Kato Propagator

Adiabatic theorem of the quantum mechanics states that, when the perturbation of the system is slow enough, starting from the instantaneous eigenstate of H_0, it passes through the next eigenstates of H_t $\forall t$. Kato proved this statement [25] even for the degenerate systems, unlike Bohm and Fock whose proof rely on the fact that the spectrum is discrete and non-degenerate.

We here give the derivation of the Kata propagotor, due to adiabatic transformation. Using the notation from Ref. [25], we can consider the general differential equation of the form,

$$\dot{X}(t) = -iA(t)X(t) \tag{5.26}$$

with $iA(t) = -[\dot{P}, P]$. Here A is the generator of the adiabatic evolution. Eq. (5.26) resembles with the time-dependent Schrodinger equation. Assume that $U_k(t)$ solves the above equation with the inital value $U_k(0) = 1$. Then the most general solution of this differential equation can be written as $X(t) = U(t)X(0)$ with $X(0)$ being the inital value. Since $U_k(t)$ also solves the equation, we can write

$$\begin{aligned} \dot{U} &= -iAU \\ \dot{U^\dagger} &= iU^\dagger A^\dagger. \end{aligned} \tag{5.27}$$

Using the definition of A,

$$\begin{aligned} -iA^\dagger &= P\dot{P} - \dot{P}P \\ &= -[\dot{P}, P]. \end{aligned} \tag{5.28}$$

Hence, A is hermitian by definition.

Using the definition of the projection operator such that $P^2(t) = P(t)$ and differentiating both sides yield

$$\begin{aligned} \dot{P}P + P\dot{P} &= \dot{P} \\ P\dot{P}P + PP\dot{P} &= P\dot{P} \\ P\dot{P}P + P\dot{P} &= P\dot{P} \\ \Rightarrow P\dot{P}P &= 0. \end{aligned} \tag{5.29}$$

Multiplying definition of A from the left by projection operator

$$\begin{aligned} iPA &= -P\dot{P}P + P\dot{P} \\ &= P\dot{P}. \end{aligned} \tag{5.30}$$

Similarly, hitting from the right yields

$$\begin{aligned} iAP &= -\dot{P}PP + P\dot{P}P \\ &= -\dot{P}P. \end{aligned} \tag{5.31}$$

Subtracting Eq. (5.30) from Eq. (5.31) and using the fact $\dot{P}P + P\dot{P} = \dot{P}$,

$$iPA - iAP = \dot{P} \Rightarrow i[P, A] = \dot{P}. \tag{5.32}$$

Now considering the operator PU and differentiating this operator yields,

$$\begin{aligned} \dot{PU} &= \dot{P}U + P\dot{U} \\ &\overset{Eq.(5.32)}{=} i[P, A]U - PiAU \\ &= iPAU - iAPU - PiAU \\ &= -iAPU. \end{aligned} \tag{5.33}$$

We can see that Eq. (5.33) has the exact form of Eq. (5.26), and using the shortened notation in the form $K = PU$, K is also solution of Eq. (5.26). Using the same logic as $X(t) = U(t)X(0)$ is being a solution, $K(t) = U(t)K(0)$ is also a solution. Since we define $K(t) = P(t)U(t)$, then

$$P(t)U(t) = U(t)P(0) \tag{5.34}$$

holds, as $K(0) = P(0)U(0)$ and $U(t)K(0) = U(t)P(0)U(0) = U(t)P(0)$ with $U(0) = 1$. We can also write, with using the definition of K(t)

$$\begin{aligned} K(t) &= P(t)U(t) \\ &= P(t)P(t)U(t) \\ &= P(t)K(t), \end{aligned} \tag{5.35a}$$

$$\begin{aligned} K(t) &= P(t)U(t) \\ &= P(t)U(t)P(0) \\ &= K(t)P(0). \end{aligned} \tag{5.35b}$$

Hence, we showed that, $P(t)K(t) = K(t)P(0)$, which is one of the most important results of Kato's adiabatic theorem, implying that if a system at $t = 0$ in its instantaneous ground state, it will pass through the corresponding instantaneous ground state at some time t, with the evolution generated by Kato propagator K.

5.1.2 Kato Propagator and non-Abelian Berry Connection

We can also write that, using Eq. (5.26)

$$K(t) = e^{-i\int_0^{t'} A(t)dt}. \tag{5.36}$$

In order to evaluate the propagator, we can use Euler method to discretize Eq. (5.26) and since $K(t)$ is a solution of the equation, we can write,

$$\begin{aligned} K(t_i) - K(t_{i-1}) &= \left[\left(P(t_i) - P(t_{i-1})\right) P(t_{i-1}) - P(t_{i-1}) \left(P(t_i) - P(t_{i-1})\right)\right] K(t_{i-1}) \\ &= P(t_i)K(t_{i-1}) - K(t_{i-1}) - P(t_{i-1})P(t_i)K(t_{i-1}) + K(t_{i-1}) \\ &= P(t_i)K(t_{i-1}) - P(t_{i-1})P(t_i)K(t_{i-1}). \end{aligned} \tag{5.37}$$

In order to massage the right hand side of the Eq. (5.37), we take the derivative of the both sides of $P(t_{i-1})K(t_{i-1}) = K(t_{i-1})$, and plug $P(t_i)K(t_{i-1}) = K(t_i) + K(t_{i-1}) - P(t_{i-1})K(t_i)$ to Eq. (5.37),

$$\begin{aligned} K(t_i) - K(t_{i-1}) &= P(t_i)K(t_{i-1}) - P(t_{i-1})K(t_i) - K(t_{i-1}) + P(t_{i-1})K(t_i) \\ &\Rightarrow K(t_i) = P(t_i)K(t_{i-1}). \end{aligned} \tag{5.38}$$

Therefore, Eq. (5.38) can be solved in terms of the Kato propgator in the continuum limit as,

$$K(t) = \lim_{n\to\infty} \prod_{i=0}^{n} P(t_i). \tag{5.39}$$

Comparing Eq. (5.39) with Eq. (2.36), in the thermodynamic limit, Kato propagator yields the Wilson loop.

Because of the Kramers' theorem, degenerate energy levels arise such that non-Abelian Berry connection has to be calculated. To do that, we assume two degenerate states, with energy ϵ_n. In the adiabatic limit, the states evolve to

$$|\Psi_{n\beta}(t)\rangle = e^{\frac{-i}{\hbar}\oint_0^{t'} \epsilon_n(t)} \sum_{\alpha} |n\alpha\rangle\, \Gamma_{\alpha\beta(t)}, \tag{5.40}$$

where α and β are degenerate states and $\Gamma_{\alpha\beta}$ is called Berry rotation matrix. As the energy levels are degenerate, Berry connection is now a matrix, instead of a scalar. Solving the time-dependent Schrodinger equation using the state at Eq. (5.40),

$$
\begin{aligned}
H\left|\Psi_{n\beta}(t)\right\rangle &= ih\frac{\delta}{\delta t}\left|\Psi_{n\beta}(t)\right\rangle \\
\epsilon_n(t)e^{\frac{-i}{h}\oint_0^{t'}\epsilon_n(t)dt}\sum_\alpha\left|n\alpha\right\rangle\Gamma_{\alpha\beta(t)} &= ih\frac{\delta}{\delta t}\left[e^{\frac{-i}{h}\oint_0^{t'}\epsilon_n(t)dt}\sum_\alpha\left|n\alpha\right\rangle\Gamma_{\alpha\beta(t)}\right] \\
\epsilon_n(t)e^{\frac{-i}{h}\oint_0^{t'}\epsilon_n(t)dt}\sum_\alpha\left|n\alpha\right\rangle\Gamma_{\alpha\beta(t)} &= \epsilon_n(t)e^{\frac{-i}{h}\oint_0^{t'}\epsilon_n(t)dt}\sum_\alpha\left|n\alpha\right\rangle\Gamma_{\alpha\beta(t)} \\
&\quad +ihe^{\frac{-i}{h}\oint_0^{t'}\epsilon_n(t)dt}\frac{\delta}{\delta t}\left[\textstyle\sum_\alpha\left|n\alpha\right\rangle\Gamma_{\alpha\beta(t)}\right] \\
0 &= \frac{\delta}{\delta t}\left[\textstyle\sum_\alpha\left|n\alpha\right\rangle\Gamma_{\alpha\beta(t)}\right] \\
&= \sum_\alpha\left(\tfrac{\delta}{\delta t}\left|n\alpha\right\rangle\right)\Gamma_{\alpha\beta}(t)+\sum_\alpha\left|n\alpha\right\rangle\frac{\delta\Gamma_{\alpha\beta}}{\delta t} \\
\frac{\delta\Gamma_{\gamma\beta}}{\delta t} &= -\sum_\alpha\left(\left\langle n\gamma\right|\tfrac{\delta}{\delta t}\left|n\alpha\right\rangle\right)\Gamma_{\alpha\beta}(t).
\end{aligned}
\tag{5.41}
$$

Defining the vector valued non-Abelian Berry connection as

$$
A_{\gamma\alpha}(t) = i\left\langle n\gamma\right|\frac{\delta}{\delta t}\left|n\alpha\right\rangle. \tag{5.42}
$$

Writing the Eq. (5.41) with using the definition of Eq. (5.42)

$$
\frac{\delta\Gamma_{\gamma\beta}}{\delta t} = i\sum_\alpha A_{\gamma\alpha}(t)\Gamma_{\alpha\beta}. \tag{5.43}
$$

Since the summation ranges in α, we can further simplify it to,

$$
\frac{\Gamma(t+dt)-\Gamma(t)}{dt} = \Gamma'(t) \tag{5.44}
$$

then, we can approximate $\Gamma(t+dt)$ as

$$
\begin{aligned}
\Gamma(t+dt) &= \Gamma(t)+idtA(t)\Gamma(t) \\
&\approx e^{idtA(t)}\Gamma(t).
\end{aligned}
\tag{5.45}
$$

Hence, we can solve it as,

$$\Gamma(t) = \mathcal{P} e^{i \oint dt A(t)} \tag{5.46}$$

with $\Gamma(0) = 1$ and $\mathcal{P}$ is path-ordering operator since non-Abelian Berry connection is a matrix valued function. Numerical calculation of the Eq. (5.46) is straightforward. Assume that, we choose $\lambda(t)$ to change slowly such that it obeys the adiabatic limit. Then, choosing a closed path $\lambda(0) = \lambda(m)$

$$\begin{aligned} \left(e^{id\lambda A(\lambda)}\right)_{\alpha\beta} &= \mathbb{1} + id\lambda A_{\alpha\beta}(\lambda) \\ &= \langle \alpha, \lambda | \beta, \lambda \rangle - d\lambda \langle \alpha, \lambda | \frac{d}{d\lambda} | \beta, \lambda \rangle \end{aligned} \tag{5.47}$$

where we use $\delta_{\alpha\beta}$ for the first term of the right-hand side. Using the fact that $\frac{d}{d\lambda} \langle \alpha, \lambda | \beta, \lambda \rangle = 0 = \langle \frac{d}{d\lambda} \alpha, \lambda | \beta, \lambda \rangle + \langle \alpha, \lambda | \frac{d}{d\lambda} \beta, \lambda \rangle$. Thus, we can change the second term of the right-hand side of the Eq. (5.47).

$$\begin{aligned} \left(e^{id\lambda A(\lambda_m)}\right)_{\alpha\beta} &= \langle \alpha, \lambda_m | \beta, \lambda_m \rangle + d\lambda \langle \frac{d}{d\lambda} \alpha, \lambda_m | \beta, \lambda_m \rangle \\ &= \langle \alpha, \lambda_{m+1} | \beta, \lambda_m \rangle . \end{aligned} \tag{5.48}$$

Hence, in the diagonalized form, the Berry rotation matrix can be written as,

$$\Gamma = \begin{bmatrix} e^{i\gamma_1} & \dots & 0 \\ \vdots & \ddots & \\ 0 & & e^{i\gamma_n} \end{bmatrix} \tag{5.49}$$

the dimensions of the matrix depends on the number of degenerate states. Hence, Berry phase can be found as $\det(\Gamma)$.

Using Eq. (5.39), then, we can find Berry rotation matrix in terms of Kato propagator as,

$$\begin{aligned} \Gamma_{\alpha\beta}(0) &= \langle \alpha(0) | K | \beta(0) \rangle \\ \Gamma_{\alpha\beta}(t) &= \langle \alpha(t) | K | \beta(0) \rangle . \end{aligned} \tag{5.50}$$

Now, returning back to Eq. (5.25) and taking the exponential of it, we have

$$
\begin{aligned}
e^{i2\pi P^I} &= e^{i\int_0^\pi A(k)dk}\frac{Pf[B(\pi)]}{Pf[B(0)]}, \\
\nu &= e^{i\int_0^\pi A(k)dk}\frac{Pf[B(\pi)]}{Pf[B(0)]}.
\end{aligned}
\tag{5.51}
$$

We already established the first term of the right-hand side of the Eq. (5.51) in the Berry rotation matrix discussion, which is nothing but the determinant of the Kato propagator in the chosen basis. We should note that, path ordering operator $\mathcal{P}$ orders k point such that, it starts from π and ends in 0. We, then, investigate the $\mathbb{Z}_2$ invariant of the spinful system with rashba spin-orbit coupling.

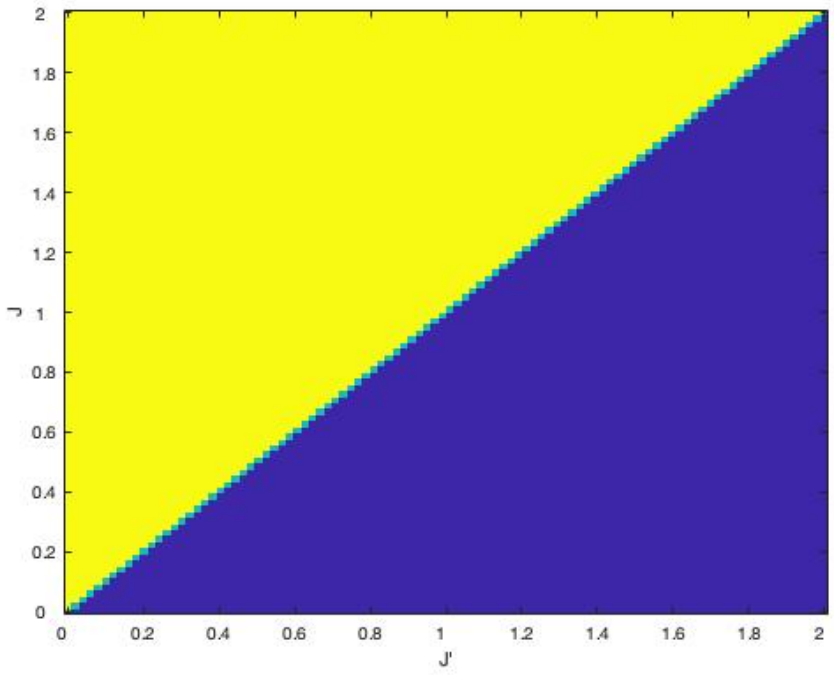

Figure 5.2: Topological invariant for spinful SSH model with rashba spin-orbit coupling as a function of J and J' at $K = 1$ and$\lambda_r = 0.1$. Blue region corresponds to non-trivial topology, whereas yellow color is trivial. Cyan color represents the gap closure.

As we know that $\mathbb{Z}_2$ invariant has only two distinct topological phases, we also show this in Fig. (5.2). As expected, gap closure occurs at $J = J'$.

Chapter 6

Conclusion

Throughout the thesis, we investigated the extensions of SSH model and calculation of topological index of corresponding model. For the topological index, we used the table given in [3], [13], where three discrete symmetries has to be known to determine the index. We showed that, although adding real next nearest neighbor give rise to topologically trivial case, as in case of Ref. [21], on-site potential gives topologically non-trivial phase due to the inversion symmetry. In the literature [26], [27], [28], Berry phase or polarization is generally used to determine the topological behavior of the system. However, we showed that extending the SSH model by adding one extra off-diagonal term, preserving the $\mathbb{Z}$ index, polarization fails to distinguish different phases. Thus, using winding number for $\mathbb{Z}$ is the most convenient. Using the ideas of Duncan Haldane [2], we changed the next nearest neighbor hopping from real to complex, thus, broke time-reversal symmetry. The alteration of real to complex hopping also changed the topological index from $\mathbb{Z}$ to $\mathbb{Z}_2$ and we showed that polarization can be used to distinguish two distinct states. For these investigations, we always ignored the distance between the sublattices. Assigning the distance of $\frac{p}{q}$ with p and q are being co-primes, we found that, to preserve periodicity of the system, we have to extend the Brillouin zone by q times. Such an extension has an effect in the parameter space. For non-trivial topology, we observed that, depending on the value of q, a knot is formed and it can be used to distinguish between trivial

and topological phases. In the last part, using the ideas of Kene-Mele [11], we added spin-orbit interaction to our model. This addition gave rise to DIII type of Hamiltonian, in which its topological indeix is $\mathbb{Z}_2$ in 1d. Using the time-reversal polarization[26], [29] and with the help of the Kato propagator, we found the $\mathbb{Z}_2$ topological index, as the hopping constants change.

Bibliography

[1] A. Altland and M. R. Zirnbauer, "Nonstandard symmetry classes in mesoscopic normal-superconducting hybrid structures," *Phys. Rev. B*, vol. 55, pp. 1142–1161, Jan 1997.

[2] F. D. M. Haldane, "Model for a quantum hall effect without landau levels: Condensed-matter realization of the "parity anomaly"," *Phys. Rev. Lett.*, vol. 61, pp. 2015–2018, Oct 1988.

[3] C.-K. Chiu, J. C. Y. Teo, A. P. Schnyder, and S. Ryu, "Classification of topological quantum matter with symmetries," *Rev. Mod. Phys.*, vol. 88, p. 035005, Aug 2016.

[4] C. C. Adams, *The Knot Book: An Elementary Introduction to the Mathematical Theory of Knots*. American Mathematical Society, 2004.

[5] K. v. Klitzing, G. Dorda, and M. Pepper, "New method for high-accuracy determination of the fine-structure constant based on quantized hall resistance," *Phys. Rev. Lett.*, vol. 45, pp. 494–497, Aug 1980.

[6] D. J. Thouless, M. Kohmoto, M. P. Nightingale, and M. den Nijs, "Quantized hall conductance in a two-dimensional periodic potential," *Phys. Rev. Lett.*, vol. 49, pp. 405–408, Aug 1982.

[7] M. V. Berry, "Quantal phase factors accompanying adiabatic changes," *Proc. R. Soc. Lond.*, vol. 392, pp. 45–57, Mar 1984.

[8] J. Zak, "Berry's phase for energy bands in solids," *Phys. Rev. Lett.*, vol. 62, pp. 2747–2750, Jun 1989.

[9] R. D. King-Smith and D. Vanderbilt, "Theory of polarization of crystalline solids," *Phys. Rev. B*, vol. 47, pp. 1651–1654, Jan 1993.

[10] R. Resta, "Macroscopic polarization in crystalline dielectrics: the geometric phase approach," *Rev. Mod. Phys.*, vol. 66, pp. 899–915, Jul 1994.

[11] C. L. Kane and E. J. Mele, "Z_2 topological order and the quantum spin hall effect," *Phys. Rev. Lett.*, vol. 95, p. 146802, Sep 2005.

[12] B. A. Bernevig, T. L. Hughes, and S.-C. Zhang, "Quantum spin hall effect and topological phase transition in hgte quantum wells," vol. 314, no. 5806, pp. 1757–1761, 2006.

[13] A. P. Schnyder, S. Ryu, A. Furusaki, and A. W. W. Ludwig, "Classification of topological insulators and superconductors in three spatial dimensions," *Phys. Rev. B*, vol. 78, p. 195125, Nov 2008.

[14] C. Li and A. Miroshnichenko, "Extended ssh model: Non-local couplings and non-monotonous edge states," *Physics*, vol. 1, no. 1, pp. 2–16, 2018.

[15] R. Resta, "Manifestations of berrys phase in molecules and condensed matter," *Journal of Physics: Condensed Matter*, vol. 12, pp. R107–R143, Feb 2000.

[16] W. P. Su, J. R. Schrieffer, and A. J. Heeger, "Solitons in polyacetylene," *Phys. Rev. Lett.*, vol. 42, pp. 1698–1701, Jun 1979.

[17] R. Shankar, "Topological insulators – a review," 2018.

[18] R. Jackiw and C. Rebbi, "Solitons with fermion number ," *Phys. Rev. D*, vol. 13, pp. 3398–3409, Jun 1976.

[19] A. W. W. Ludwig, "Topological phases: classification of topological insulators and superconductors of non-interacting fermions, and beyond," *Physica Scripta*, vol. T168, p. 014001, dec 2015.

[20] S. Kivelson, "Wannier functions in one-dimensional disordered systems: Application to fractionally charged solitons," *Phys. Rev. B*, vol. 26, pp. 4269–4277, Oct 1982.

[21] L. Li, Z. Xu, and S. Chen, "Topological phases of generalized su-schrieffer-heeger models," *Phys. Rev. B*, vol. 89, p. 085111, Feb 2014.

[22] B. Hetényi, Y. Pulcu, and S. Doğan, "Calculating the polarization in bipartite lattice models: Application to an extended su-schrieffer-heeger model," *Phys. Rev. B*, vol. 103, p. 075117, Feb 2021.

[23] A. A. Aligia and G. Ortiz, "Quantum mechanical position operator and localization in extended systems," *Phys. Rev. Lett.*, vol. 82, pp. 2560–2563, Mar 1999.

[24] J. C. Budich and E. Ardonne, "Topological invariant for generic one-dimensional time-reversal-symmetric superconductors in class diii," *Phys. Rev. B*, vol. 88, p. 134523, Oct 2013.

[25] T. Kato, "On the adiabatic theorem of quantum mechanics," *J. Phys. Soc. Jpn.*, vol. 5, pp. 435–439, Mar 1950.

[26] B. A. Bernevig and T. L. Hughes, *Topological Insulators and Topological Superconductors*. Princeton University Press, 2013.

[27] J. K. Asbóth, L. Oroszlány, and A. Pályi, *A Short Course on Topological Insulators*. Springer International Publishing, 2016.

[28] C. Kane, "Topological band theory and the $\mathbb{Z}_2$ invariant," *Elsevier*, vol. 6, 2013.

[29] L. Fu and C. L. Kane, "Time reversal polarization and a Z_2 adiabatic spin pump," *Phys. Rev. B*, vol. 74, p. 195312, Nov 2006.

Appendix A

Winding Number

Following the definition of Ref. [27], the winding number is given by,

$$\nu = \frac{1}{2\pi}\int \left(\tilde{d}(k) \times \frac{d}{dk}\tilde{d}(k)\right)_z dk \tag{A.1}$$

where $\tilde{d}(k) = \frac{d}{|d|}$. Note that, the cross product is in the z-direction, implying no z-dependence of the Hamiltonian or σ_z term. Writing the cross product in an open form,

$$\begin{aligned}
\left(\tilde{d}(k) \times \frac{d}{dk}\tilde{d}(k)\right) &= \frac{(dx, dy, 0)}{|d|} \times \frac{d}{dk}\left(\frac{dx, dy, 0}{|d|}\right) \\
&= \left(\frac{d_x}{|d|}\left(\frac{d}{dk}\frac{d_y}{|d|}\right) - \frac{d_y}{|d|}\left(\frac{d}{dk}\frac{d}{d_x}\right)\right)_{d_z} \\
&= \frac{d_x}{|d|}\left(\frac{d'_y}{|d|} + d_y\frac{d}{dk}\frac{1}{|d|}\right) - \frac{d_y}{|d|}\left(\frac{d'_x}{|d|} + d_x\frac{d}{dk}\frac{1}{|d|}\right) \\
&= \frac{d_x d'_y}{d^2} - \frac{d_y d'_x}{d^2}.
\end{aligned} \tag{A.2}$$

As we can write $d^2 = (d_x - id_y)(d_x + id_y)$, and defining $h(k) = d_x - id_y$,

$$
\begin{aligned}
(d_x + id_y)\frac{d}{dk}(d_x - id_y) &= d_x d'_x + d_y d'_y - i(d_x d'_y - d_y d'_x) \\
\Rightarrow d_x d'_y - d_y d'_x &= i(d_x + id_y)\frac{d}{dk}(d_x - id_y) - i(d_x d'_x + d_y d'_y)
\end{aligned}
\tag{A.3}
$$

Hence, we can write winding number as

$$
\nu = \frac{i}{2\pi}\int \frac{i(d_x + id_y)\frac{d}{dk}(d_x - id_y)}{d^2}dk - \frac{i}{2\pi}\int \frac{d_x d'_x + d_y d'_y}{d^2}dk \tag{A.4}
$$

Second integral of the Eq. (A.4) can be evaluated as,

$$
-\frac{i}{2\pi}\int_{-\pi}^{\pi} \frac{d_x d'_x + d_y d'_y}{d_x^2 + d_y^2}dk = -\frac{i}{4\pi}\log\left(d_x^2 + d_y^2\right)|_{-\pi}^{\pi} = 0 \tag{A.5}
$$

as $(d_x^2 + d_y^2) = h^2(k)$ and $h^2(-\pi) = h^2(\pi)$. Thus, we left with the first integral of the Eq. (A.4),

$$
\begin{aligned}
\nu &= \frac{i}{2\pi}\int \frac{i(d_x + id_y)\frac{d}{dk}(d_x - id_y)}{d^2}dk \\
&= \frac{i}{2\pi}\int \frac{(d_x + id_y)\frac{d}{dk}(d_x - id_y)}{(d_x + id_y)(d_x - id_y)}dk \\
&= \frac{i}{2\pi}\int \frac{\frac{d}{dk}(d_x - id_y)}{(d_x - id_y)}dk \\
&= \frac{i}{2\pi}\int \frac{\frac{d}{dk}(h(k))}{h(k)}dk \\
&= \frac{i}{2\pi}\int dk\frac{d}{dk}\log h(k)
\end{aligned}
\tag{A.6}
$$

which is equal to Eq. (2.60)

Appendix B

Relating the Position Expectation to Berry Phase

As we have shown that,

$$\langle x \rangle = \int \Psi \hat{x} \Psi dx$$

is ill defined due to unboundedness of the position operator. Because of the periodic nature of the crystal, we can define an operator in the form

$$\eta = \exp\left(-2\pi i x/L\right) \tag{B.1}$$

The usage of η operator is advantageous over x for couple of reasons. First of all, it is bounded, thus, one can get a sensible result for any large L. The other advantage is that, we can label any position operator uniquely since Eq. (B.1) is actually a phase angle

$$\langle x \rangle = \frac{iL}{2\pi} ln \left\langle \eta \right\rangle . \tag{B.2}$$

Hence, calculating the η, we have

$$\begin{aligned}\langle \Psi_{n,k}| \eta |\Psi_{n,k'}\rangle &= \frac{1}{N}\int_0^{Na} dx U_{n,k}U_{n,k'} \exp i(k'-k-2\pi/L)x \\ &= \delta_{k,k+\frac{2\pi}{L}} \int_0^a dx U_{n,k}U_{n,k+\frac{2\pi}{L}} \\ &= \delta_{k,k+\frac{2\pi}{L}} \langle U_{n,k}|U_{n,k+\frac{2\pi}{L}}\rangle .\end{aligned} \tag{B.3}$$

Using the Taylor expansion, we can write

$$\langle U_{n,k}|U_{n,k+\frac{2\pi}{L}}\rangle = 1 + \frac{2\pi}{L}\langle U_{n,k}|\nabla_k U_{nk}\rangle . \tag{B.4}$$

So that we arrive the following equation,

$$\langle \Psi_{n,k}| \eta |\Psi_{n,k'}\rangle \simeq 1 + \frac{2\pi}{L}\langle U_{n,k}|\nabla_k U_{nk}\rangle . \tag{B.5}$$

Using the Eq. (B.2), we have

$$\begin{aligned}\langle \Psi_{n,k}| x |\Psi_{n,k+\frac{2\pi}{L}}\rangle &= \frac{iL}{2\pi}\ln\langle \Psi_{n,k}| \eta |\Psi_{n,k+\frac{2\pi}{L}}\rangle \\ &\simeq i\langle U_{n,k}|\nabla_k U_{nk}\rangle\end{aligned} \tag{B.6}$$

for large L, $k+\frac{2\pi}{L} \approx k$ such that we can write the Eq. (B.6) as

$$\langle \Psi_{n,k}| x |\Psi_{n,k}\rangle = i\langle U_{n,k}|\nabla_k U_{n,k}\rangle . \tag{B.7}$$

Appendix C

A Way of Calculating the Berry Phase of the System

While calculating the Berry phase of the system, there are two options: Using $|\Psi_{nk}\rangle$ and $|u_{nk}\rangle$. The former one, so called the Bloch eigenstates has many problems. As we can write the phase mismatch between the two states as $\langle\Psi_{n,k}|\Psi_{n,k+\delta}\rangle$, which can be written as,

$$\int \Psi^*_{n,k}(x)\Psi^*_{n,k+\delta}(x) = \int e^{i\delta x}u_{n,k}(x)u^*_{n,k+\delta}(x) \tag{C.1}$$

with δ is a small crystal momentum. Because of the phase that is appeared in the right-hand side of the Eq. (C.1), the choices of the unit cells, [0,a] or [-a/2] to [a/2] would give different results. The other problematic part of using Bloch eigenstates is that, derivative operator is ill defined. Using the Bloch's theorem, we can write

$$\nabla_k\Psi_{n,k}(x) = \nabla_k e^{ikx}u_{n,k}(x) = e^{ikx}\left[ixu_{n,k}(x) + \nabla_k u_{n,k}(x)\right]. \tag{C.2}$$

As it can be seen that there is a linear dependence on the position x, hence, as x approaches the infinity, Eq. (C.2) becomes ill-defined. Thus, we have to stick with the cell periodic functions. Because the system is periodic, we have to ensure

that, $\Psi_{n,k=0}(x) = \Psi_{n,k=2\pi}(x)$ (periodic gauge) where we take the lattice constant as unity. Hence, using the Bloch's theorem, we can write

$$u_{n,k=2\pi}(x) = e^{-2\pi ix} u_{n,k=0}(x). \tag{C.3}$$

As it can be seen that, there is a phase mismatch between the cell periodic function at $k = 0$ and $k = 2\pi$. This phase mismatch is meaningless when the orbitals in the original SSH model is on top of each other, meaning that the distance between the A and B sublattices are disregarded. However, it is important when there is distance dependence. The subtle point is that, one does not need to extend the Brillioun zone q times if the distance between the sublattices are p/q and the presented method will be used. Therefore, one-band systems, we can write the Berry Phase of the system as

$$\begin{aligned} \phi &= \langle u_1|u_2\rangle \langle u_2|u_3\rangle ... \langle u_{N-1}|u_N\rangle \\ &= \langle u_1|u_2\rangle \langle u_2|u_3\rangle ... \langle u_{N-1}|e^{-2\pi ix}|u_1\rangle \end{aligned} \tag{C.4}$$

where N^{th} point and 1^{st} corresponds to same Bloch eigenstate due to the periodicity of the system. For more than one-band systems, Wilson loop aproach should be used.